# Design and crystal structure of a native-like HIV-1 envelope trimer that engages multiple broadly neutralizing antibody precursors *in vivo*

Max Medina-Ramirez[1*], Fernando Garces[2*], Amelia Escolano[3], Patrick Skog[4], Steven W. de Taeye[1], Ivan Del Moral-Sanchez[1], Andrew T. McGuire[5], Anila Yasmeen[6], Anna-Janina Behrens[7], Gabriel Ozorowski[2], Tom L.G.M. van den Kerkhof[1, 8], Natalia T. Freund[3], Pia Dosenovic[3], Yuanzi Hua[2], Alexander D. Gitlin[3], Albert Cupo[6], Patricia van der Woude[1], Michael Golabek[6], Kwinten Sliepen[1],Tanya Blane[4], Neeltje Kootstra[8], Mariëlle J. van Breemen[1], Laura K. Pritchard[7], Robyn L. Stanfield[2], Max Crispin[7], Andrew B. Ward[2], Leonidas Stamatatos[5], Per Johan Klasse[6], John P. Moore[6], David Nemazee[4], Michel C. Nussenzweig [3, 9], Ian A. Wilson[2#], Rogier W. Sanders[1,6#]

[1] Department of Medical Microbiology, Academic Medical Center, University of Amsterdam, Amsterdam, The Netherlands
[2] Department of Integrative Structural and Computational Biology, Scripps CHAVI-ID, IAVI Neutralizing Antibody Center and Collaboration for AIDS Vaccine Discovery (CAVD), The Scripps Research Institute, CA 92037, La Jolla, USA
[3] Laboratory of Molecular Immunology, The Rockefeller University, New York, NY 10065, USA
[4] Department of Immunology and Microbial Science, Scripps CHAVI-ID, The Scripps Research Institute, La Jolla, CA 92037, USA
[5] Seattle Biomedical Research Institute, Seattle, WA 98109, USA
[6] Department of Microbiology and Immunology, Weill Medical College of Cornell University, New York, NY 10012, USA
[7] Oxford Glycobiology Institute, Department of Biochemistry, University of Oxford, Oxford, UK
[8] Department of Experimental Immunology, Academic Medical Center, University of Amsterdam, Amsterdam, The Netherlands
[9] Howard Hughes Medical Institute
* These authors contributed equally to the work
[#] Correspondence to Rogier W. Sanders (r.w.sanders@amc.uva.nl) or Ian A. Wilson (wilson@scripps.edu).

Abbreviations used: NAb, neutralizing antibody; Env, envelope glycoprotein; gl, germline; GT, germline targeting.

**SUMMARY**

Induction of broadly neutralizing antibodies (bNAbs) by HIV-1 envelope glycoprotein (Env) immunogens would be a major advance towards an effective vaccine. A critical step in this process is the activation of naïve B cells expressing germline (gl) antibody precursors that have the potential to evolve into bNAbs. Here, we reengineered the BG505 SOSIP.664 glycoprotein to engage gl-precursors of bNAbs that target either the trimer apex or the CD4 binding site. The resulting BG505 SOSIP.v4.1-GT1 trimer binds multiple bNAb gl-precursors *in vitro*. Immunization experiments in knock-in mice expressing gl-VRC01 or gl-PGT121 show that this trimer activates B cells *in vivo*, resulting in the secretion of specific antibodies into the sera. A crystal structure of the germline-targeting trimer at 3.2 Å resolution in complex with neutralizing antibodies 35O22 and 9H+109L reveals a native-like conformation and the successful incorporation of design features associated with binding of multiple gl-bNAb precursors.

## INTRODUCTION

An effective HIV vaccine will likely require the elicitation of protective titers of broadly neutralizing antibodies (bNAbs). The envelope glycoprotein (Env) on the virion surface is the only relevant target for bNAbs and, hence, is the main focus for antibody-based vaccine strategies. Approximately 30-50% of infected individuals eventually develop bNAbs (Burton and Mascola, 2015; Hraber et al., 2014; Mascola and Haynes, 2013; van Gils and Sanders, 2013), and passive immunization studies have shown that various bNAbs can protect macaques from experimental challenge (Barouch et al., 2013; Gautam et al., 2016; Hessell et al., 2009; Shingai et al., 2014). However, it has not yet been possible to induce bNAbs by vaccination. Even eliciting neutralizing antibodies (NAbs) with narrow-specificity against neutralization-resistant (Tier-2) primary viruses has been challenging, but is nevertheless possible (Escolano et al., 2017; Sanders and Moore, 2017; Sanders et al., 2015).

The Env spike on HIV-1 virions is a metastable complex consisting of three gp120 and three gp41 subunits associated through non-covalent interactions. Soluble trimers of the SOSIP design (de Taeye et al., 2016; Sanders and Moore, 2017) that faithfully mimic the native spike have yielded valuable insights into the structural details of how Env functions and the bNAb epitopes it presents (Ward and Wilson, 2017). SOSIP trimers have induced strong and consistent autologous Tier 2 NAb responses in rabbits and somewhat weaker responses in macaques (de Taeye et al., 2015; Klasse et al., 2016; Sanders et al., 2015). A major goal is now to devise a strategy to broaden these narrow specificity NAb responses into ones resembling bNAbs. To

74 develop more sophisticated vaccination regimens will require combining our
75 increasing knowledge of Env structure with an understanding of bNAb development.
76 During HIV-1 infection, bNAbs usually emerge over time from an initial,
77 narrowly focused, autologous NAb response to transmitted/founder viruses that are
78 susceptible to gl-bNAbs binding (Bonsignori et al., 2017). This process requires high
79 levels of somatic mutation (Escolano et al., 2017) mediated by multiple cycles of viral
80 escape from antibody pressure generating new variants that, in turn, drive additional
81 antibody affinity maturation (Doria-Rose et al., 2014; Liao et al., 2013). Can Env
82 immunogens be designed to mimic this process (Haynes et al., 2012; Klein et al.,
83 2013a; Medina-Ramirez et al., 2017; Sanders and Moore, 2017)? To do so would
84 require specific targeting and activation of B-cell lineages that could eventually evolve
85 into bNAb-producing clones. One approach involves engineering an immunogen to
86 recognize the germline (gl) forms of bNAbs and thereby prime specific B-cell lineages
87 (Dosenovic et al., 2015; Escolano et al., 2016; Haynes et al., 2012; Jardine et al., 2013;
88 Jardine et al., 2016; Jardine et al., 2015; Klein et al., 2013b; McGuire et al., 2016; Ota et
89 al., 2012; Scharf et al., 2016; Stamatatos et al., 2017; Steichen et al., 2016). Boosting
90 with additional immunogens to guide the affinity maturation pathway may then yield
91 NAbs with the required breadth and potency (Bonsignori et al., 2017; Escolano et al.,
92 2017; Stamatatos et al., 2017). The critical priming immunogen should, therefore,
93 activate naïve B cells expressing at least one potential bNAb-precursor, and preferably
94 several. The gl-precursors for several bNAbs have been inferred by sequence analysis,
95 providing templates for guiding immunogen design (Bonsignori et al., 2011; Doria-

96 Rose et al., 2014; Jardine et al., 2013; Pancera et al., 2010; Scheid et al., 2011; Sliepen
97 et al., 2015).

98 A bNAb epitope cluster of interest is the CD4-binding site (CD4bs). The CD4
99 receptor and several sub-families of bNAbs bind to overlapping epitopes on both
100 gp120 monomers and native-like trimers. However, many antibodies that recognize
101 CD4bs-associated epitopes on the outer domain (OD) of the gp120 monomer cannot
102 do so on the trimer, due to topological constraints imposed by the trimeric
103 architecture. This subset of CD4bs antibodies is non-neutralizing (i.e., non-NAbs) for
104 Tier-2 viruses (Chen et al., 2009).

105 The VRC01-class of bNAbs, which includes VRC01 and 3BNC60, epitomizes
106 both the potential of the CD4bs and the challenges associated with the design of gl-
107 targeting immunogens for eliciting such antibodies. The presentation of the epitopes
108 for these potent bNAbs on both gp120 monomer and native trimer is now well
109 understood at the structural level (Kong et al., 2016; Scharf et al., 2016; Wu et al.,
110 2011). One key finding is how *N*-linked glycans in the loop D and V5 regions of gp120
111 impede binding of gl-bNAbs to the CD4bs (Gristick et al., 2016; Kong et al., 2016;
112 McGuire et al., 2013). Thus, whereas the mature VRC01 and 3BNC60 bNAbs bind Env
113 proteins with high affinity, the corresponding gl-bNAbs do not (Klein et al., 2013a;
114 Scheid et al., 2011; Zhou et al., 2010). An unmodified Env immunogen would not,
115 therefore, be likely to trigger the induction of these bNAb lineages. Structure-guided
116 design has successfully produced Env-based proteins with increased affinity for gl-
117 bNAbs of the VRC01-class, designated eOD-GT6/8 and 426c.TM4ΔV1-V3 (Jardine et
118 al., 2013; Jardine et al., 2016; McGuire et al., 2016; McGuire et al., 2013). These

119 immunogens were able to activate antibody responses in knock-in mice engineered to
120 express the gl-precursors of VRC01 or 3BNC60, but did not induce bNAbs (Dosenovic
121 et al., 2015; Jardine et al., 2015; McGuire et al., 2016; Tian et al., 2016). Under the
122 same conditions, native-like BG505 SOSIP.664 trimers did not initiate gl-VRC01 or gl-
123 3BNC60 antibody lineages, which is consistent with their non-reactivity with these
124 bNAb precursors *in vitro* (Dosenovic et al., 2015; Sliepen et al., 2015). However, when
125 the same trimers were tested in knock-in mice transgenic for the mature 3BNC60
126 heavy chain (HC), they selected an appropriate light chain (LC) from the antibody
127 repertoire, which enabled induction of NAbs with some breadth (Dosenovic et al.,
128 2015). The above observations underpin our hypothesis that an engineered trimer
129 that has an appropriate affinity for a gl-bNAb could initiate a B-cell lineage that can be
130 guided towards evolution of bNAbs by boosting with one or more rationally chosen
131 Env trimers.

132 Another suitable target for gl-targeting Env immunogen design is the Env
133 trimer apex that is recognized by bNAbs such as CH01, PG9/PG16,
134 PGT145/PGDM1400 and VRC26 (Bonsignori et al., 2011; Doria-Rose et al., 2014; Sok
135 et al., 2014; Walker et al., 2009). The trimer-apex epitopes are attractive vaccine
136 design targets because apex-directed bNAbs derived from several different germline
137 genes emerge comparatively early and frequently during HIV-1 infection. Moreover,
138 although the latter bNAbs require high levels of somatic hypermutation for optimal
139 breadth and potency, the extent of mutation is lower than for VRC01-class antibodies
140 (Doria-Rose et al., 2014; Klein et al., 2013a; Walker et al., 2011; Walker et al., 2009;
141 West et al., 2012). These properties suggest that inducing similar bNAbs in humans by

vaccination may be easier than inducing bNAbs against other epitopes. As trimer-apex bNAbs recognize gp120-V2 epitopes that are either highly influenced by, or completely dependent on, the quaternary structure of the trimer, a trimer-based immunogen is probably required to initiate these lineages. Some native-like trimers, including BG505 SOSIP.664, can engage trimer-apex gl-bNAbs (Andrabi et al., 2015; Gorman et al., 2016; Sliepen et al., 2015), providing a strong foundation for structure-guided design improvements to yield higher affinity immunogens.

Here, we describe an engineered trimer variant, BG505 SOSIP.v4.1-GT1 (GT1: germline-targeting trimer version 1), with improved capacity for binding gl-bNAbs that target the trimer-apex and the CD4bs epitopes.

## RESULTS

### Design of the BG505 SOSIP.v4.1-GT1 trimer

Our goal was to engineer a variant of the BG505 SOSIP.664 Env trimer with enhanced binding to inferred gl-bNAbs, including those targeting the CD4bs and the V1V2-apex **Table S1**). To remove impediments to trimer binding of CD4bs gl-bNAbs, we eliminated potential *N*-linked glycosylation sites (PNGS) in loop D and V5 via N276D and N462D substitutions, respectively (Jardine et al., 2013; Joyce et al., 2013; Li et al., 2011; McGuire et al., 2013; Wu et al., 2011). We also removed two additional PNGS at positions 386 in the mannose patch (via N386D) (Jardine et al., 2013; Li et al., 2011; Sanders et al., 2008) and at 197 in the bridging sheet (via S199A) (Li et al., 2011).

164 Finally, we created a favorable contact between loop D and the VRC01 light chain (via
165 T278R), and also stabilized loop 5 (via G471S) (Jardine et al., 2013).

166 To obtain insights into V1V2-apex epitopes, we measured the ability of gl-
167 versions of PG9, PG16 and PGT145 (and, for comparison, the mature bNAbs) to
168 neutralize a panel of 30 viruses, and then analyzed the V2 sequences of the
169 neutralization-sensitive and -resistant subgroups (**Table S2**). The panel included a
170 BG505.T332N-LAI chimeric infectious molecular clone (IMC) derived from the BG505
171 isolate (data not shown), as well as BL035 and Q23 clade A Env-pseudotyped viruses
172 that have epidemiologic and genetic links to BG505 (Bonsignori et al., 2011; Neilson et
173 al., 1999; Wu et al., 2006) (**Table S2**). The remaining viruses were 27 clade B clinical
174 isolates obtained 1-12 months after infection from patients enrolled in the
175 Amsterdam Cohort Studies on HIV/AIDS (ACS) that developed moderate to strong
176 neutralization breadth (Euler et al., 2011; Euler et al., 2010; Lynch et al., 2015; van
177 den Kerkhof et al., 2013) (**Table S2**). The rationale for choosing these 27 viruses was
178 that early Env sequences from patients whose neutralization response broadened
179 over time might be markedly more reactive with gl-bNAbs than Env sequences shaped
180 by the antibody response in chronically infected people (Doria-Rose et al., 2014; Liao
181 et al., 2013).

182 BG505.T332N-LAI IMC was resistant to all three gl-bNAbs at the maximum
183 concentration tested while BL035 was neutralized (>50% inhibition) by gl-PG9 and
184 gl-PG16, and Q23 was sensitive to all three. Four of the ACS clade B viruses (D16928,
185 D12950, H19829 and H19793) were neutralized by all three gl-bNAbs and six more
186 by two of them (**Table S2**). We then aligned the Env V2 amino-acid sequences from

187 the viruses neutralized by two or three gl-bNAbs to identify possible determinants of
188 gl-bNAb engagement. Relevant sequence changes were then introduced, alone or in
189 combination, into the BG505 sequence to construct new SOSIP trimer variants for
190 assessment of gl-bNAb reactivity (see below). Among these changes was a 7-residue
191 deletion in the gl-bNAb-sensitive Q23 virus compared to the resistant BG505 virus,
192 also from clade A (**Tables S3 and S4**). We also flagged two BL035 residues (Y173H
193 and S174A) and three Q23 residues (K169R, V181I, and Q183P). (**Tables S3 and S4**).
194 Several other potential influences on gl-bNAb reactivity were identified when the ACS
195 clade B V2 sequences were analyzed, but only one had a beneficial effect when tested
196 experimentally, specifically the introduction of an NTS sequon (G188N, N189T,
197 E190S) from the D12950 sequence (**Table S3** and data not shown). We also noted that
198 a non-BG505 peptide that had nanomolar affinity for gl-PG9 and gl-CH01 had a R178K
199 change relative to the BG505 sequence (Aussedat et al., 2013).

200 Taken together, sequence changes relevant to the trimer-apex and CD4bs
201 epitopes are outlined in **Fig. 1A, B**. Various changes were introduced, singly or in
202 combination, into D7324- or His-tagged BG505 SOSIP constructs. The designs also
203 incorporated one or both of the A316W and E64K substitutions, which confer
204 additional stability to trimers designated as SOSIP.v4.1 when both substitutions are
205 combined (de Taeye et al., 2015) (**Fig. 1A, B; Tables S3-S5**). The variant trimers were
206 expressed by transient transfection of HEK293T cells, and the unpurified culture
207 supernatants were used in a D7324 or a Ni-NTA/His-tag capture ELISA, as
208 appropriate, to obtain preliminary estimates of expression levels (2G12 binding),
209 native-like trimer formation (PGT145 binding) and gl-bNAb reactivity (**Tables S3 and**

**S4**). The most promising new constructs were then further purified by PGT145 for more extensive evaluation (**Table S5**). The final outcome was that the BG505 SOSIP.664 construct was modified by 9 substitutions in V2 (K169R, Y173H, S174A, R178K, V181I, Q183P, G188N, N189T, E190S), a 7-residue deletion in V2, 6 sequence changes around the CD4bs (S199A, N276D, T278R, N386D, N462D, T471S), and the E64K and A316W substitutions for stability. The resulting trimers were expressed efficiently and bound several gl-bNAbs targeting both the trimer-apex and the CD4bs (**Tables S3, S4**)(see below). The construct including all the above 18 modifications is designated BG505 SOSIP.v4.1-GT1, or for convenience, the GT1 trimer.

The PGT145-purified GT1 trimer was fully cleaved as assessed by BN-PAGE and reducing and non-reducing SDS-PAGE (Data not shown), and predominantly native-like when visualized by negative-stain electron microscopy (NS-EM) (**Fig. 1C**). Its midpoint of thermal denaturation ($T_m$), as assessed by differential scanning calorimetry (DSC), was 67.7°C (**Fig. 1D**), which is almost identical to that of the BG505 SOSIP.664 prototype (Sanders et al., 2013). Finally, the glycan profile of the GT1 trimer was dominated by oligomannose glycans, similar to those of the parental SOSIP.664 and SOSIP.v4.1 trimers as well as native trimers on virions, but with a slightly higher ratio of $Man_8$:$Man_9$ (**Fig. 1E** and **Table S6**) (Behrens et al., 2016).

**BG505 SOSIP.v4.1-GT1 trimers bind multiple gl-bNAbs**

In a capture ELISA, PGT145-purified GT1 trimers bound several trimer-apex gl-bNAbs (gl-PG9, gl-PG16 and gl-CH01) more strongly (2-5 fold) than did the SOSIP.v4.1 precursor (**Figs. 2A** and **S1B**). Three CD4bs-directed VRC01-class gl-bNAbs (gl-

VRC01, gl-NIH45-46 and gl-PGV19) bound well to the GT1 trimers and two others (gl-12A12 and gl-CH31) did so at an intermediate level, which contrasts with their undetectable binding to the unmodified trimers (**Figs. 2A** and **S1B**). We observed very weak binding of the CD4bs-directed gl-CH103 to the SOSIP.v4.1 and GT1 trimers on ELISA (**Fig. S1B**), but only weak binding to GT1 on SPR (**Fig. S2**). gl-1NC9 or gl-3BNC60 binding was unmeasurable. There was no detectable or only minimal binding of the mature, CD4bs-directed non-NAbs b6 and F105 to either trimer (**Figs. S1A** and **S3**). We previously reported that gl-3BC315 (against a conformational epitope on gp41) bound to the unmodified BG505 SOSIP.664 trimer (Sliepen et al., 2015). The epitope for this gl-bNAb was preserved on the GT1 variant (**Figs. 2A** and **S1B**).

We analyzed antibody binding by surface plasmon resonance (SPR) by using immobilized His-tagged trimers and antibodies (IgG) as the analyte, and by applying a bivalent model to the data (Yasmeen et al., 2014). Both the mature and gl versions of PG16 had higher affinities, i.e. lower $K_{d1}$ values, for GT1 trimers than for SOSIP.v4.1; the extent of binding (stoichiometries; $S_m$ values) to GT1 was also greater than to SOSIP.v4.1 trimers for both versions of PG16 (**Fig. 2B, Table S7**). The higher affinities, i.e. lower $K_{d1}$ values, were attributable to both higher on- and lower off-rate constants ($k_{on1}$ and $k_{off1}$). Similarly, the mature versions of the CD4bs-specific bNAbs VRC01, 3BNC60, and CH103 had greater on-rate constants and extents of binding to GT1 than to SOSIP.v4.1 trimers, although their off-rate constants were too low to be determined ($k_{off1}$ $<10^{-5}$ (1/s)). The gl versions of these bNAbs did not bind detectably to SOSIP.v4.1 trimers but did bind to GT1, although only gl-VRC01 had an affinity strong enough to be quantified (**Fig. S2 and Table S7**). Another mature bNAb to the CD4bs, 1NC9,

likewise had a higher on-rate, $k_{on1}$, (although also a higher $k_{off1}$ and lower affinity) and stoichiometry of binding to GT1 than to SOSIP.v4.1 trimers. However, the gl-1NC9 version failed to bind to any trimer. The CD4bs non-NAbs b6 and F105 reacted weakly with BG505 SOSIP.664 trimers but did not bind the SOSIP.v4.1 variant detectably, (**Fig. S3**). We confirmed that b6 and F105 were also non-reactive with the GT1 trimer, which implies that the modifications did not adversely affect the geometry of its CD4bs and associated epitopes. Finally, the mature bNAb PGT121 bound strongly and with comparable affinities to its N332/V3-base epitope on the SOSIP.v4.1 and GT1 trimers but its gl version bound to neither trimer (**Table S7**).

Thus, the SPR analyses showed that the modifications that created the GT1 trimer enabled or enhanced the binding of gl versions of PG16 and three CD4bs bNAbs (VRC01, CH103, 3BNC60), in particular by improving their on-rate constants and stoichiometries, while also improving the binding of some mature bNAbs.

**Crystal structure of the BG505 SOSIP.v4.1-GT1 trimer**

Inserting, deleting or substituting individual residues could have ramifications on the overall protein conformation, including the reorganization or rearrangement of quaternary epitopes such as those found at the Env trimer apex. Here, we sought to investigate, at the atomic level, whether the 17 amino-acid substitutions and 7-residue deletion in the GT1 trimer perturbed its structure compared to its SOSIP.664 prototype (Garces et al., 2015; Julien et al., 2013; Pancera et al., 2014). Guided by the 3.0-Å crystal structure of the BG505 SOSIP.664-N137A trimer (Garces et al., 2015), we removed the PNGS at position 137 (via N137A) from the GT1 construct for

crystallization. The resulting trimer was combined with 35O22 Fab to stabilize the gp120-gp41 interface and promote crystal packing (Pancera et al., 2014), and with 9H+109L Fab, an N332/V3-base-directed antibody that binds with high affinity when the N137 glycan is absent (Garces et al., 2015)(Note that 9H is a putative heavy-chain precursor of the PGT121 family). We were then able to determine the crystal structure of GT1 at 3.2 Å resolution (**Fig. 3A**).

A structural alignment of the GT1 and prototype SOSIP.664 trimers showed a Cα root-mean-square deviation (RMSD) of 0.28 Å (**Table S8**), indicating that the gl-targeting design changes did not substantially alter the native trimer conformation (**Fig. 3A**). The structure allowed us to visualize the location of the engineered substitutions (**Fig. 3B**, **3C**), and thus supported the rationale for the design (see below). Of note is the extensive electron density for W316, which was introduced to decrease V3-mobility and increase trimer stability (**Fig. 3D**) (de Taeye et al., 2015). The side-chain of W316 could adopt more than one rotamer (which is difficult to define at this resolution) and is positioned between the side chains of R308 and Y318, providing a possible explanation for how it stabilizes the V3. Moreover, use of 9H+109L allowed comparison of its epitope and mode of binding with 3H+109L, a proposed precursor of 9H in the PGT121 heavy-chain lineage (**Fig. S4A**) (Garces et al., 2015). Both antibodies adopt the same angle of approach, and the glycans in and around their epitopes at positions N332, N301 and N156 have highly conserved conformations in the two structures (**Fig. S4A and B**); the same is true of the conserved GDIR motif at the base of V3, a key component of the PGT121 and PGT128 epitopes (**Fig. S4B**) (Garces et al., 2014). A slight conformational change in the V1 tip

(**Fig. S4B**) might be attributed to the deletion of the N137 glycan, as previously observed (Garces et al., 2015).

**Models of the BG505 SOSIP.v4.1-GT1 trimer with VRC01-class gl-bNAbs and PG9**

To understand in atomic detail how the engineered changes increase the affinity of the GT1 trimer for gl-bNAbs, we superimposed the structures of several Env proteins in complex with VRC01-class precursors onto the GT1 trimer structure. We also created an *in silico* model of the GT1 trimer + PG9 complex utilizing information from the crystal structure of mature PG9 in complex with a scaffolded V1V2 domain from the ZM109 isolate (see below) (McLellan et al., 2011).

The superimposition of the eOD-GT6 + gl-VRC01 complex (PDB: 4JPK) (Jardine et al., 2013) onto the GT1 trimer structure confirms how removal of *N*-linked glycans at N197, N276, and N462 most likely reduce potential clashes with gl-VRC01 (**Fig. 4C**). This outcome is consistent with the ELISA data (**Table S3**). The N276D substitution also allows formation of a hydrogen bond (H-bond) with the antibody TyrL91 (**Fig. 4B**), the T278R change creates an additional contact with SerL28 (**Fig. 4B**) (Jardine et al., 2013), and G471S appears to have a stabilizing effect on the V5 loop by a facilitating a new intra-gp120 H-bond with Thr455 (**Fig. 4B**). Superimposing the 426c.TMΔ1-3 gp120 + gl-NIH45-46 complex (PDB: 5IGX) (Scharf et al., 2013; Scharf et al., 2016) onto the GT1 trimer highlights the extensive overlap between the contact residues of gl-VRC01 and gl-NIH45-46 (**Fig. S4C-E**).

In the 1.8-Å crystal structure of the scaffolded ZM109 V1V2 domain with mature PG9 (PDB: 3U2S), Lys169 (in V2 strand C) forms an H-bond with a sulfated

tyrosine (Tys) at position 100G in HCDR3 (TysH100G) (McLellan et al., 2011). Our *in silico* modeling suggests that Arg169 of the GT1 trimer can also form such an H-bond, but the guanidinium of Arg169 can form stronger electrostatic interactions with the sulfated TysH100G of PG9 (Woods et al., 2007). The V2 contact with TysH100G is important because the presence of the HCDR3 YYD-motif encoded by the germline *D3-3*01* gene could help the GT1 trimer to select Abs that contain this motif (Andrabi et al., 2015). Furthermore, Arg169 might also form an additional H-bond with a neighboring (non-sulfated) TyrH100E residue (**Fig. 4A**). These additional interactions might explain why the GT1 trimer has enhanced affinity for PG9 and gl-PG9. The model also sheds light on the Y173H substitution. In the PG9/ZM109-V1V2 reference complex, Asn173 forms an H-bond with TyrH100K (McLellan et al., 2011). In BG505 SOSIP.664, Tyr173 would clash with TyrH100K (data not shown), but the Y173H substitution in the GT1 trimer would eliminate this clash and enable a H-bond to form with TyrH100K (**Fig. 4A**) in mature PG9, and also with TrpH100K in gl-PG9.

In crystal structures of BG505 SOSIP.664, which contain the full-length V2 loop, 9 V2 residues starting from Asn185 and including two PNGS (PDB: 4TVP) (Julien et al., 2013; Pancera et al., 2014) are unresolved. We hypothesize that this flexible region inhibits interactions with HCDR3 of mature and precursor bNAbs, such as PG9, and therefore the 7 amino-acid deletion in this region of V2 in the GT1 trimer might alleviate that inhibition.

### ***In vitro*** **and** ***in vivo*** **activation of B cells expressing gl-VRC01**

We next evaluated whether the BG505 SOSIP.664 and GT1 trimers could activate B-cell lines expressing the germline version of VRC01. The GT1 trimers did indeed activate gl-VRC01 B cells, whereas the parental SOSIP.664 trimers were ineffective (**Fig. 5A**). Although both trimers activated B cells expressing the mature VRC01, the GT1 variant was better (**Fig. 5A**). Thus, the improved gl-VRC01 binding properties of the GT1 trimer translate into superior activation of B cells carrying a gl-VRC01 BCR.

To assess whether the above *in vitro* observation is predictive of what happens when a GT1 trimer encounters a naïve VRC01-class B cell *in vivo*, we immunized mice expressing the inferred germline *IgH* gene of VRC01; i.e., $gl_H$-VRC01 knock-in mice (Jardine et al., 2015). One group of mice received GT1 trimers and, for comparison, two others were given SOSIP.664 or SOSIP.v4.1 trimers. The outcome of the experiment was determined by measuring binding antibody responses in sera, via a capture ELISA based on His-tagged versions of the immunogen trimers and mutants thereof in which relevant epitopes were inactivated. Binding antibody responses were significantly higher in the mice immunized with GT1 trimers when measured against the GT1 trimer than SOSIP.v4.1 ($P=0.003$) or the GT1-D368R mutant ($P=0.01$). Thus, a substantial fraction of the antibody response was against epitopes that are better displayed on the GT1 trimers and that involve residue D368 in the CD4bs (**Figs. 5B [left panel], C and S5A**). We also used a mutant trimer SOSIP.v4.1-N276D/T278R/Δ7 that included two substitutions in loop D (N276D and T278T) to enhance accessibility of the CD4bs and a 7-residue deletion in V2. These changes are also present in the GT1 trimer and allowed moderate binding to gl-VRC01 (**Fig. S1C and Table S5**). The binding responses in the GT1 trimer-immunized mice were significantly higher when

measured against this mutant compared to SOSIP.v4.1 (P=0.003), which is further evidence for the elicitation of antibodies that recognize the CD4bs (**Figs. 5B [left panel] and S5A**).

The antibody responses in mice immunized with the SOSIP.v4.1 or SOSIP.664 control trimers were substantially lower than in the GT1 trimer-immunized animals, irrespective of the trimer used in the detection ELISA (**Fig. 5B**). The reduced response was particularly striking for the SOSIP.664 immunized animals. In these two groups of control animals, the binding antibody responses were not statistically significantly affected by GT1 substitutions (GT1 *vs.* SOSIP.v4.1), by reduction of VRC01 contacts (GT1 *vs.* GT1-D368R) or by enhanced exposure of the CD4bs (SOSIP.v4.1 *vs.* SOSIP.v4.1-N276D/T278R/Δ7) (**Fig. 5B [middle and right], and C**). The implication is that the antibodies elicited in these mice predominantly recognize epitopes that are not specific for the CD4bs, i.e. irrelevant off-target responses, probably stemming from the remaining B cells that express mouse BCRs (Jardine et al., 2015).

### *In vivo* activation of B cells expressing gl-PGT121

To determine whether GT1 trimers could trigger gl-antibody responses to epitopes outside the CD4bs, we immunized knock-in mice expressing the predicted germline *IgH* gene of the N332/V3-base directed bNAb PGT121; i.e. $gl_H$-PGT121 knock-in mice (Escolano et al., 2016). These mice were given either the GT1 trimer or, for comparison, SOSIP.v4.1. The antibody responses among the 11 GT1 trimer-immunized mice were very variable, but were significantly higher when measured against the GT1 trimer than against a mutant trimer containing four substitutions that

393 knock-out the PGT121 epitope (GT1-N137A/N332A/N301A/H330A; P=0.007). They
394 were also higher when measured against GT1 trimers than SOSIP.v4.1 (P=0.01). The
395 implication is that, in at least some of the mice, the antibody responses to the GT1
396 trimer are targeting the PGT121 epitope (**Figs. 5D [left panel], E and S5B**). These
397 results are striking in light of the undetectable binding of the GT1 trimer to gl-PGT121
398 in ELISA and SPR assays assays (**Fig. S1B, S2** and **Table S7**), but in agreement with a
399 previous study showing that PGT121 responses could be initiated *in vivo* with a
400 protein that had no measureable affinity to gl-PGT121 (Escolano et al., 2016; Steichen
401 et al., 2016). The SOSIP.v4.1 control trimer induced a low level of trimer binding
402 antibodies in the $gl_H$-PGT121 knock-in mice, but there was no difference in their
403 recognition of the GT1 trimer, the SOSIP.v4.1 trimer or the GT1-
404 N137A/N332A/N301A/H330A (**Fig. 5D, E)** designed to knock out PGT121 binding
405 (**S1D**). It is, therefore, likely that these antibodies are not specific for the PGT121
406 epitope but are off-target responses.
407 We conclude that the BG505 SOSIP.v4.1-GT1 trimer can activate B cells
408 expressing germline versions of two different bNAbs to two different epitope clusters
409 under *in vivo* conditions.
410
411 **DISCUSSION**
412 The concept of targeting gl-antibody precursors is now acknowledged as an important
413 strategy for HIV-1 Env vaccines that are intended to induce bNAbs in humans
414 (Escolano et al., 2017; Medina-Ramirez et al., 2017; Sanders and Moore, 2017; Scheid
415 et al., 2009; Stamatatos et al., 2017; Verkoczy et al., 2017; Xiao et al., 2009b). Thus,

Env immunogens must be designed to engage and activate naïve B cells expressing germline Abs that have the potential to evolve into a bNAb. Subsequent boosting by a different or modified immunogen may then help drive the somatic hypermutation events required to evolve bNAbs. How then can Env immunogens be designed to target germline versions of bNAbs? Env proteins tend to react poorly with gl-bNAbs as they are based on sequences that have been shaped by the antibody response to HIV-1 infection and the particular virus that initiated the response is often not known (Doria-Rose et al., 2014; Haynes et al., 2012; Klein et al., 2013b; Liao et al., 2013; Lynch et al., 2015; Mouquet et al., 2010; Scheid et al., 2009; Xiao et al., 2009a; Xiao et al., 2009b; Zhou et al., 2010). Accordingly, Env proteins must be redesigned to create immunogens that can bind gl-bNAbs with high affinity *in vitro* and, by extension, activate the analogous naïve B cells *in vivo*.

Our approach was based on modifying native-like recombinant SOSIP trimers based on the BG505 sequence. The BG505 SOSIP.664 trimer and its more stable SOSIP.v4.1 derivative bind multiple bNAbs *in vitro* and elicit autologous Tier-2 NAbs in animals (de Taeye et al., 2015; Klasse et al., 2016; Sanders et al., 2015). They do not, however, induce bNAb responses. Moreover, although the BG505 SOSIP.664 trimer binds to gl-precursors of the PG9/16, CH01 and 3BC315 bNAbs *in vitro*, it fails to react with several others including all those tested from the VRC01-class (Sliepen et al., 2015).

Here, we describe the reengineering of the BG505 SOSIP.664 trimer to increase affinity for gl-precursors of multiple bNAb lineages. The key elements of the design strategy involve removing steric clashes that hinder germline binding, and creating

favorable new antibody-antigen contacts that promote selection of the appropriate gl-bNAb. The high-resolution 3.2 Å structure of the resulting GT1 trimer, particularly when compared to the SOSIP.664 structure, permits a mechanistic dissection of how it engages gl-bNAbs. The GT1 trimer is fully native-like, has biochemical, biophysical and expression properties comparable to its SOSIP.664 and SOSIP.v4.1 precursors and can be purified to structural homogeneity by bNAb affinity chromatography. These characteristics offer a practical path to producing the GT1 trimer as an immunogen for further testing in animals and, perhaps, eventually in humans.

On ELISA, the GT1 trimer bound 2-5 fold more strongly to three gl-bNAbs against trimer-apex epitopes (gl-PG9, gl-PG16, gl-CH01) when compared to its precursors. The GT1 trimer also gained the ability to bind strongly to CD4bs gl-bNAbs gl-VRC01, gl-NIH45-46 and gl-PGV19, moderately to gl-12A12 and weakly but detectably to gl-CH31 and gl-CH103 (**Figs. 2A, B and S1B**). We tested the immunogenicity of the GT1 and control trimers in knock-in mice expressing the gl-precursors for two different bNAbs: VRC01 to the CD4bs and PGT121 to the N332/V3-base cluster. Antibodies with characteristics consistent with the respective gl-bNAbs were induced in both models in response to the GT1 trimer immunogen, as judged by their ELISA reactivity with the same trimer and mutants with sequence changes affecting the target epitope. In contrast, the SOSIP.v4.1 or SOSIP.664 control trimers did not induce antibodies with these properties (**Figs. 5B-E and S5**).

The GT1 trimer was not designed to activate gl-PGT121 B cells and did not bind to gl-PGT121 in ELISA and SPR experiments. Nevertheless, the GT1 trimer, but not the parental trimer, initiated an epitope-specific response *in vivo*. Thus, (the lack of)

462 binding by SPR does not necessarily predict the outcome of *in vivo* experiments
463 (Escolano et al., 2016). We do not know how the GT1 trimer activates gl-PGT121 B
464 cells, but the changes made in GT1 might have enhanced access to the PGT121 epitope
465 *in vivo*.

466 Of note is that, in SPR analyses, GT1 resembles the unmodified SOSIP.v4.1
467 trimer by binding with high affinity to mature CD4bs bNAbs, such as VRC01, but not
468 reacting with CD4bs antibodies F105 and b6 that are non-NAbs against Tier-2 viruses.
469 The retention of trimerization-induced constraints on the CD4bs epitopes suggests
470 that the GT1 trimer may have the selectivity to induce desired lineages (e.g., for
471 VRC01-like bNAbs) without activating "off-target" lineages (e.g., non-NAbs like F105
472 and b6) *in vivo*. This property could be highly advantageous because the angle of
473 approach to the trimer of several bNAb lineages analyzed to date appears to be
474 established at the germline stage, with only minor changes during affinity maturation
475 (Fera et al., 2014; Garces et al., 2015; Jardine et al., 2013; Scharf et al., 2016; Zhou et
476 al., 2013). Accordingly, off-target lineages might never yield bNAbs. In summary, the
477 conformational selectivity offered by SOSIP.v4.1-GT1 trimers may help to determine
478 the appropriate selection and development of CD4bs bNAb lineages.

479 Two other germline-targeting Env immunogen designs, the 426c and eOD
480 proteins, have been specifically constructed to induce precursors of the VRC01-family
481 of CD4bs bNAbs (Stamatatos et al., 2017). However, as the CD4bs regions of the 426c
482 and eOD proteins are not constrained by trimerization, they may also present non-
483 NAb epitopes. It is not yet known whether the presence of such "off-target" epitopes

484 matters from the perspective of inducing VRC01 gl-bNAbs that can then be shaped by
485 boosting with a second immunogen, such an Env trimer.

486 As noted, the GT1 trimer was engineered to bind inferred gl-bNAbs targeting
487 several epitope clusters, not just a single one (Dosenovic et al., 2015; Escolano et al.,
488 2016; Jardine et al., 2013; Jardine et al., 2015; Sok et al., 2016; Steichen et al., 2016),
489 and it has the appropriate antigenicity properties *in vitro*. These design features may
490 broaden the human repertoire of gl-bNAb precursors that can be targeted and
491 increase the probability that at least one family of gl-bNAb B cells will be activated *in*
492 *vivo*. Could the current GT1 trimers be further modified to present more gl-bNAb
493 epitopes, such as those at the gp120-gp41 interface? Could a "universal germline-
494 targeting trimer" be created? Or would it be better to design a suite of different
495 trimers that individually target a specific gl-bNAb cluster? These questions can only
496 be addressed experimentally. For example, removing multiple glycans that clash with
497 a variety of gl-bNAbs may have adverse structural consequences and alter glycan
498 processing. Furthermore, improving the targeting of one epitope cluster may also
499 adversely affect a neighboring or even a distant one.

500 While these are encouraging initial indicators of appropriate immunogenicity,
501 the limitations of knock-in mouse models must be recognized. For example, in the
502 knock-in mice, a far higher proportion of B cells express the gl-bNAb receptor than
503 would be the case in humans. Thus, to achieve a similar response in humans, it may be
504 necessary to further increase an Env immunogen's affinity for the germline antibodies
505 being targeted while preventing potential competition from unwanted binders

(Escolano et al., 2017; Medina-Ramirez et al., 2017; Sanders and Moore, 2017; Stamatatos et al., 2017).

This new germline-targeting trimer is suitable for further evaluation as an immunogen to gauge its abilities to induce gl-bNAb lineages and the specificity with which it does so. In all likelihood, it will need then to be combined with carefully designed boosting immunogens to ensure that a broadly neutralizing antibody response is appropriately shaped and productively matured.

## MATERIALS AND METHODS

### Construction of a BG505.T332N-LAI chimeric molecular clone

The molecular clone of LAI was used as the backbone (Peden et al., 1991). This clone contains a unique Sal1 restriction site 434 nucleotides upstream of the *env* start codon and a unique BamH1 site at the codons specifying amino acids G751 and S752 in LAI gp160 (HxB2). A DNA fragment was synthesized containing the LAI sequences between the Sal1 site and the *env* start codon, followed by the BG505.T332N *env* sequences up to the BamH1 site (Genscript, Piscataway, NJ) and cloned into the LAI molecular clone backbone using Sal1 and BamH1. The resulting molecular clone encodes the complete BG505.T332N gp160 sequence, except for the C-terminal 106 amino acids of the cytoplasmic tail, which are derived from LAI gp160. The resulting virus was able to infect TZM-bl cells and replicate in PBMCs (Data not shown).

### Neutralization assays

The virus neutralization activities of antibodies targeting the trimer apex were assessed using the TZM-bl cell assay as described elsewhere (Sanders et al., 2015). The PG9, PG16 and PGT145 bNAbs were tested at single concentrations of 5 μg/ml (mature versions) and 50 μg/ml (germline versions). All experiments were performed in triplicate. The assay endpoint (percentage neutralization) was calculated relative to the extent of HIV-1 infection measured in the absence of antibody.

**Trimer expression and purification**

Env proteins were expressed by transient transfection of adherent HEK293T cells (incubated for 48h) or suspension FreeStyle™ 293F cells (Invitrogen) (incubated for 6 days), as described previously (Julien et al., 2013; Sanders et al., 2013). Env proteins were purified from culture supernatants by PGT145-affinity chromatography (de Taeye et al., 2015). Trimer cleavage and purity was assessed using SDS-PAGE and BN-PAGE analyses (Data not shown) (Sanders et al., 2013).

**Env trimer design and mutagenesis**

To create the BG505 SOSIP.v4.1-GT1 trimer, 17 individual point substitutions and a 7 amino-acid deletion were introduced into the BG505 SOSIP.664 construct (**see Fig. 1 A, B**) using the Quikchange site-directed mutagenesis kit (Agilent, Stratagene, Santa Clara, CA). Specific epitope knock-out substitutions (D368R for VRC01 and N137A/N332A/N301A/H330A for PGT121), as well as substitutions that removed the N276 glycan and 7 amino acids from V2 (N276D/T278R/Δ7), were introduced using the same method. His-tagged or D7324-tagged versions of the same or similar trimers

were also produced (de Taeye et al., 2015; Sanders et al., 2013). His- and D7324-tagged trimers were used in ELISA, His-tagged trimers in B-cell activation assays, and SPR (see below), whereas NS-EM, DSC, and crystallography studies were performed with non-tagged trimers. The presence or absence of these epitope tags does not influence the structure of the trimer (Sanders et al., 2013). The purities of trimers were assessed using BN- and SDS-PAGE followed by staining with Coomassie blue as described previously (data not shown)(Sanders et al., 2013). The biochemical and biophysical assays for Env trimer characterization have all been published elsewhere (de Taeye et al., 2015).

**ELISA for trimer antigenicity**

We adapted an ELISA protocol as previously described (Derking et al., 2015). Briefly, His-tagged trimers, either pure (3.5 µg/ml in TBS buffer) or in unpurified HEK293T cell culture supernatant (His- and D7324-tagged) (supplemental information), were immobilized (100 µl/well) for 2 h on 96-well Ni-NTA ELISA plates (Qiagen) or 96-well ELISA plates coated overnight with D7324 antibody (Aalto Bioreagents, Dublin, Ireland). After washing away excess protein with TBS, the wells were blocked for 30 min with Casein/TBS (Thermo Scientific, 37532). Serial dilutions of each antibody were prepared in Casein/TBS at a starting concentration of 1 µg/ml and added to the plate (100 µl/well) (for lower affinity Abs, the starting concentration was 50 µg/ml). The dilution factor for all antibodies was 1:3 except for gl-CH103 which was 1:2. Excess antibody was washed away after 2h and anti-human horseradish peroxidase

(HRP)-conjugated antibody (diluted in Casein/TBS 1:3000) added for 45 min before binding was quantified. All steps were carried out at room temperature (RT).

**Analysis of total N-glycan profile by HILIC-UPLC**

N-linked glycans were enzymatically released by in-gel PNGase F digestion from trimers resolved by non-reducing SDS-PAGE. The released glycans were fluorescently labelled with 2-aminobenzoic acid (2-AA) and analyzed as previously described (Pritchard et al., 2015).

**B cell activation assays**

DG75 B cells were transfected by electroporation with a plasmid expressing the mature VRC01 IgG BCR. After 24h, the cells were loaded with Fluo-4 direct $Ca^{2+}$ indicator dye and then stained with an anti-IgG antibody labeled with BV421 to identify transduced cells. Baseline Fluo-4 fluorescence was measured for 30 s after which the indicated recombinant Env proteins were added to a final concentration of 1 μM. Changes in Fluo-4 fluorescence were monitored for an additional 210 s. Ionomycin was then added to a final concentration of 6.5 nM for an additional 60 s of fluorescence monitoring. Maximum Fluo-4 fluorescence ($Max_{FL}$) was established by averaging the fluorescence changes recorded during the last 10 s of monitoring. The percent of maximum Fluo-4 fluorescence at each time point, t, was determined using the formula: (Fluorescence at t-$Min_{FL}$)/($Max_{FL}$-$Min_{FL}$) x 100. This analysis was performed on both transfected and untransfected cells simultaneously. The background Fluo-4 fluorescence signal from the BCR-negative cells was subtracted

from that of the BCR-positive population at each time point. The same analysis was performed for DG75 B cells stably transduced to express the gl-VRC01 BCR (McGuire et al., 2016).

**Differential scanning calorimetry**

Differential scanning calorimetry (DSC) was used to determine the thermostability of purified trimers, as described previously (de Taeye et al., 2015; Pugach et al., 2015).

**Surface Plasmon Resonance**

Surface Plasmon Resonance (SPR) was performed as previously described with immobilized His-tagged trimers and antibodies (IgG) as the analytes; binding parameters were derived by applying a bivalent model (Yasmeen et al., 2014). The bivalent model dissects the initial monovalent from the subsequent bivalent binding, as previously validated by comparing IgG with Fabs and trimers at different densities (Yasmeen et al., 2014). Here we used the standard level of trimer immobilization, $R_L$ = 500 RU, which falls in the range of trimer densities on virions that have been estimated and typically gives a low degree of bivalency (Klein and Bjorkman, 2010; Yasmeen et al., 2014). Overall, the bivalent component reproducibly represented a minority of the binding events. Here, we converted the units of the bivalent constants $k_{on2}$ and $K_{d2}$ from (1/RUs)) and (RU) to (1/Ms) and (nM), by taking into account the reaction volume on the SPR chip and the specific signal per mass unit of analyte. These considerations give the formula $1\ 1/(\mathrm{RUs}) \sim 100 \cdot \mathrm{M_A}\, 1/(\mathrm{Ms})$, where $\mathrm{M_A}$ is the molar mass of the analyte, as described (Karlsson et al., 1995). Although this conversion

conveniently confers the same dimension to the mono- and bivalent on-rate constants, it should be born in mind that the unoccupied paratopes do not diffuse freely and their local concentrations in relation to the epitope-presenting trimers immobilized to dextran remain unknown. Therefore, the constants for bi- and monovalent binding are not directly comparable in spite of the conversion. Nevertheless, the $K_{d1}$ values were lower than the $K_{d2}$ values in all cases but one: BG505 SOSIP.664 and mature PG16 antibody, for which the two constants were similar (52 vs. 30 nM). A strong bivalent contribution to the binding would manifest itself as substantially lower $K_{d2}$ than $K_{d1}$ values. The low degree of bivalency was also evident from comparisons that do not depend on the above conversion: component analyses of each binding cycle modeled bivalently and a comparison of the T values, indicating significance of the fitted parameter, for the $k_{on1}$ and $k_{on2}$ values (the off-rate constants being less amenable to comparison since $k_{off1}$ was frequently below detection. The T values for $k_{on1}$ were consistently >10 with a minimum = 63; the T value for $k_{on2}$ was <10 in ~25% of the cases; the minimum = 3.1. Such weak bivalency is to be expected at a trimer density that is in the range of what occurs on virion surfaces (Klein and Bjorkman, 2010). We therefore conclude that the kinetic and stoichiometric measurements that we obtained for the monovalent paratope-epitope interaction were largely unaffected by the highly limited propensity for bivalent interaction, in line with previous comparisons of Fab with IgG binding and the Langmuir with bivalent modeling (Yasmeen et al., 2014).

An advantage of using IgG rather than Fabs, apart from obviating the need for Fab production and purification of all antibodies, is a stronger signal through the 3-

642 fold greater mass, allowing detection of weak gl-bNAb binding. Furthermore, the use
643 of IgG incorporates unusual allosteric effects transmitted from the Fc portion to the
644 paratope (Crespillo et al., 2014), manifestations of asymmetries in the IgG molecules
645 (Saphire et al., 2002), and reduction in epitope accessibility on immobilized trimers by
646 the bulk of the IgG molecule (Labrijn et al., 2003).
647
648 **Negative-stain electron microscopy**
649 Negative-stain electron microscopy (NS-EM) assessed Env trimer morphology
650 following previously described procedures (de Taeye et al., 2015; Pugach et al., 2015;
651 Sanders et al., 2013).
652
653 **Mice and immunizations**
654 The $gl_H$-PGT121 mice (carrying the *Ig V(D)J* genes encoding the germline *IgH*) were
655 produced by gene targeting Albino B6 (B6 (Cg)-*Tyrc-2J*/J) embryonic stem cells. The
656 amino acid sequence of the heavy chain of gl-PGT121 (**Table S1**) was previously
657 described (Escolano et al., 2016). The constant regions of *IgH* as well as the *IgL*
658 diversity remain of mouse origin. The targeting vectors for *IgH* contained homologous
659 regions flanking mouse *D4-1* and *J4*. Recombination results in the deletion of the
660 endogenous *D4-1* and *Js* thereby minimizing rearrangement of the locus (Pelanda et
661 al., 1997; Shih et al., 2002). The $gl_H$-VRC01 knock-in mice have been described
662 elsewhere (Jardine et al., 2015).
663 Two and three independent experiments were performed using the $gl_H$-VRC01
664 and $gl_H$-PGT121 mice, respectively. Mice were immunized three times every 2-4

665 weeks intraperitoneally (i.p.) with 10μg of protein in Ribi adjuvant (Sigma-Aldrich).
666 Serum samples were collected two weeks after the third immunization. All animal
667 procedures were performed in accordance to protocols approved by The Scripps
668 Research Institute (VRC01 mice) or The Rockefeller University (all other mice)
669 IACUCs.
670
671 **ELISA for anti-trimer antibodies in mouse sera**
672 ELISAs to measure serum responses to the BG505 SOSIP variants were adapted from
673 elsewhere (Derking et al., 2015; Dosenovic et al., 2015; Yasmeen et al., 2014). In brief,
674 His-tagged antigen was captured by using Ni-NTA ELISA plates (Qiagen) or,
675 alternatively, with an anti-$His_6$-tag antibody (Abcam). Plates coated overnight with
676 anti-$His_6$-tag antibody were washed six times (PBS with 0.05% Tween 20 [Sigma-
677 Aldrich] or TBS) and blocked in blocking buffer (1xPBS with 1% milk) for 1h at RT.
678 Immediately after blocking (n.b., no blocking for Ni-NTA plates), His-tagged GT1,
679 SOSIP.v4.1 or SOSIP.664 trimer (or mutants thereof) were added at 3.5μg/ml in TBS
680 (or 2μg/ml diluted in PBS with 1% fetal bovine serum and 0.2% Tween20 for antigens
681 captured with the anti-$His_6$ antibody) to all the wells and incubated at RT for 1 or 2 h.
682 Plates were then washed and blocked for 1 h at RT. After blocking, serum samples
683 were added in PBS with 1% fetal bovine serum and 0.2% Tween20 (for antigens
684 captured with the anti-$His_6$ antibody) or 2% skim milk in TBS supplemented with
685 20% sheep serum [Biotrading] for the Ni-NTA plates) and incubated for 2 h at 37°C.
686 Sera were added at 1:100 starting dilution. Seven additional three-fold serial dilutions
687 were made. Plates were washed and incubated for 1.5 h at 37°C with an HRP-anti-

mouse IgG antibody (Jackson Laboratories) (in PBS with 0.05% Tween 20 or 2% skim milk in TBS) at a 1:5000 dilution. Plates were developed by addition of the HRP substrate, ABTS (Life Technologies) and absorbance was measured with an ELISA microplate reader (at 405nm in a FluoStar Omega [BMG Labtech] or at 450nm in a Spectrostar nano [BMG Labtech]).

**Expression and purification of proteins for x-ray crystallographic studies**

The 9H+109L and 35O22 Fabs were produced by transient transfection of FreeStyle™ 293F cells and purified by affinity chromatography using CaptureSelect LC lambda (ThermoFisher Scientific) followed by cation exchange and size exclusion chromatography (SEC) on a Superdex 200 16/60 column (GE Healthcare). The BG505 SOSIP.v4.1-GT1-N137A construct was cloned into a phMCV3 vector, expressed in FreeStyle™ 293S cells (incubated for 6 days), and trimers purified by 2G12-affinity chromatography followed by SEC. The purities of trimers and Fabs were assessed using SDS-PAGE followed by staining with Coomassie blue as described previously (Sanders et al., 2013).

**Crystallization and data collection**

Multiple combinations of Fabs and BG505 SOSIP.v4.1-GT1 trimers (including the substitution N137A) were assessed for complex formation in crystallization trials. Generally, Fabs and trimers were mixed in a 3.2:1 molar ratio, To increase the homogeneity of trimer:ligand complexes, a deglycosylation procedure was performed as described previously (Garces et al., 2015), followed by further SEC purification.

To facilitate crystal packing, the GT1 trimer was complexed with Fab 35O22 and Fabs from the PGT121 family, including 9H+109L and 3H+109L (Garces et al., 2015; Pancera et al., 2014). Samples of SEC-purified ternary complexes were concentrated to ~12 mg/ml and screened against 480 crystallization conditions at 4 °C using a robotic Rigaku CrystalMation system. The most successful combination, SOSIP.v4.1-GT1 in complex with Fabs 9H+109L and 35O22, was initially crystallized in JCSG Core II Suite (Qiagen) condition E12 (0.2M sodium chloride, 0.1M sodium acetate, 40% PEG 300, pH 4.5) and, after further optimization, crystals for data collection were grown in 0.2 M sodium chloride, 34% (v/v) PEG 300, and 0.1 M sodium acetate, pH 4.5. Crystals were flash cooled in liquid nitrogen using the well solution as cryoprotectant and data were collected at APS beamline 23-ID-D. Despite the best crystal producing a few strong reflections beyond 3.0 Å resolution, the final dataset was processed with HKL-2000 (Otwinowski and Minor, 1997) to 3.2 Å with an overall $R_{sym}$ of 0.11 and 100% completeness in space group $P6_3$ with unit cell parameters: $a = b = 128.0$ Å, $c = 316.1$ Å (**Table S8**) (Weiss and Hilgenfeld, 1997).

**Structure determination and refinement**

The structure was solved by molecular replacement with Phaser (Adams et al., 2010) using the BG505 SOSIP.664 structure in complex with 3H+109L and 35O22 (PDB ID:5CEZ) as the search model. Model building was carried out using Coot (Emsley and Cowtan, 2004) and refinement with phenix.refine (Adams et al., 2010) using reference model restraints calculated from structures of BG505 SOSIP.664 with 3H+109L and 35O22 (PDB ID:5CEZ) and 35O22 (PDB ID: 4TOY). The final $R_{cryst}$ and $R_{free}$ values were

27.2% and 28.5% (**Table S8**). The Fab residues were numbered according to Kabat (Kabat et al., 1991) and gp120 and gp41 residues using HxB2 numbering. Ramachandran statistics were calculated using MolProbity (Chen et al., 2010).

## Data processing and statistical analysis

The Geneious 9.0.4 and MacVector 14.0.3 programs were used for sequence analysis. Flow cytometry data was processed using FlowJo 10.0.7. GraphPad Prism 6.0f was used for data and statistical analysis by one-way ANOVA and the Tukey multi comparison test. Data were considered statistically significant at $*p \leq 0.05$.

## ACCESSION NUMBERS

Env sequence data for isolates H19463, H18969 and H19792 are available at GenBank (www.ncbi.nlm.nih.gov/GenBank), with accession numbers JF910186, EU744055 and JF910175. The coordinates and structure factors of the BG505 SOSIP.v4.1-GT1 trimer crystal structure with Fabs 35O22 and 9H+109L are being deposited in the PDB with accession number XXXX and will be available immediately upon publication.

## Online supplemental material

Fig. S1 shows representative ELISA binding curves to multiple BG505 SOSIP trimer variants using a panel of mature bNAbs and gl-bNAbs. Figs. S2 and S3 show SPR analysis of binding of bNAbs, gl-bNAbs and non-NAbs to three versions of BG505 SOSIP trimers. Fig. S4 shows structural analysis of bNAb precursor engagement to BG505 SOSIP.v4.1-GT1-N137A. Fig. S5 shows representative ELISA binding curves to

multiple BG505 SOSIP variants using sera derived from immunization of $gl_H$-VRC01 and $gl_H$-PGT121 knock-in mice. Table S1 lists the heavy and light chain sequences of the gl-bNAbs used in this study. Table S2 shows the analysis of gl-bNAb neutralization sensitivity of a panel of viruses. Tables S3 to S5 shows the relative binding capacity of a panel of three gl-bNAbs and two bNAbs to BG505 SOSIP trimer variants. Table S6 shows the percentage of $Man_{5\text{-}9}GlcNAc_2$ glycans (M5-M9) in three BG505 SOSIP trimer variants. Table S7 shows the SPR analysis of a panel of mature bNAbs and gl-bNAbs to BG505 SOSIP trimer variants. Table S8 shows the X-ray data collection and refinement statistics.

**AUTHOR CONTRIBUTIONS**

Project design by M.M.-R., F.G., A.E., I.d.M.-S., D.N., M.C.N., J.P.M., I.A.W. and R.W.S.; X-ray structure determination, computer modeling, and interpretation by F.G., M.M.-R, K.S., R.W.S, R.L.S. and I.A.W.; Design, characterization and analysis of the knock-in mice work by A.E., M.M.-R., T.B., and P.S.; Generation of knock-in mice by N.T.F., P.D., A.D.G., and P.S.; EM by G.O. and A.B.W.; Env protein mutagenesis by M.M.-R., I.d.M.-S. and F.G.; DSC experiments by M.J.v.B.; virus neutralization assays by M.M.-R and T.L.G.M.K; protein expression, analysis and purification by M.M.-R., A.C., M.G., P.v.d.W., F.G. and Y.H.; SPR data generated and modeled by A.Y. and P.J.K.; analysis of glycan profile by A.-J.B., L.K.P. and M.C.; *in vitro* B cell activation assays by A.T.M.; manuscript written or edited by M.M.-R., F.G., A.E., P.J.K., D.N., M.C.N, M.C., A.B.W., I.A.W., J.P.M. and R.W.S. All

779 authors were asked to comment on the manuscript. This is manuscript #XXXX from
780 The Scripps Research Institute.
781
782 **ACKNOWLEDGEMENTS**
783 We thank Larry Liao, Barton Haynes, William Schief, John Mascola, Pamela Bjorkman
784 and Peter Kwong for providing antibodies. We thank Judith Burger and Michael
785 Golabek for technical assistance. We thank the Amsterdam Cohort Studies on
786 HIV/AIDS (ACS) for providing 27 HIV-1 clinical isolates. The ACS is a collaboration
787 between the Amsterdam Health Service, the Academic Medical Center of the
788 University of Amsterdam, Sanquin Blood Supply Foundation, and the Jan van Goyen
789 Clinic, are part of The Netherlands HIV Monitoring Foundation and are financially
790 supported by the Center for Infectious Disease Control of The Netherlands National
791 Institute for Public Health and the Environment). Portions of the research were
792 carried out at GM/CA@APS, which has been funded in whole or in part with Federal
793 funds from the National Cancer Institute (ACB-12002) and the National Institute of
794 General Medical Sciences (AGM-12006). This research used resources of the Advanced
795 Photon Source, a U.S. Department of Energy (DOE) Office of Science User Facility
796 operated for the DOE Office of Science by Argonne National Laboratory under
797 Contract No. DE-AC02-06CH11357.
798 The authors declare no competing financial interests.
799
800 **FUNDING**

M.M.-R. is a recipient of a fellowship from the Consejo Nacional de Ciencia y Tecnologıa (CONACyT) of Mexico. R.W.S. is a recipient of a Vidi grant from the Netherlands Organization for Scientific Research (grant #917.11.314) and a Starting Investigator Grant from the European Research Council (ERC-StG-2011-280829-SHEV). This work was also supported by NIH P01 AI110657 (J.P.M., A.B.W., I.A.W. and R.W.S.), the International AIDS Vaccine Initiative through the Neutralizing Antibody Consortium SFP1849 (M.C., A.B.W. and I.A.W.), Center for HIV/AIDS Vaccine Immunology and Immunogen Discovery Grant (CHAVI-ID) UM1 AI100663 (M.C.N., R.W.S., M.C., A.B.W. and I.A.W.), NIH grant R01 AI073148 (D.N.), Collaboration for AIDS Vaccine Discovery (CAVD) grants OPP1111923 and OPP1132237 (J.P.M. and R.W.S.) and OPP1115782 (A.B.W.) from the Bill and Melinda Gates Foundation. This project has received funding from the European Union's Horizon 2020 research and innovation programme under grant agreement No. 681137 (M.C. and R.W.S.). The Amsterdam Cohort Studies on HIV/AIDS is a multi-institutional collaborative effort incorporated to The Netherlands HIV Monitoring Foundation and is financially supported by the Center for Infectious Disease Control of The Netherlands National Institute for Public Health and the Environment).

## REFERENCES

Adams, P.D., P.V. Afonine, G. Bunkoczi, V.B. Chen, I.W. Davis, N. Echols, J.J. Headd, L.W. Hung, G.J. Kapral, R.W. Grosse-Kunstleve, A.J. McCoy, N.W. Moriarty, R. Oeffner, R.J. Read, D.C. Richardson, J.S. Richardson, T.C. Terwilliger, and P.H. Zwart. 2010. PHENIX: a

824 comprehensive Python-based system for macromolecular structure solution. *Acta*
825 *Crystallogr D Biol Crystallogr.* 66:213-221.

826 Andrabi, R., J.E. Voss, C.H. Liang, B. Briney, L.E. McCoy, C.Y. Wu, C.H. Wong, P. Poignard, and
827 D.R. Burton. 2015. Identification of common features in prototype broadly
828 neutralizing antibodies to HIV envelope V2 apex to fcilitate vaccine design. *Immunity*
829 43:959-973.

830 Aussedat, B., Y. Vohra, P.K. Park, A. Fernandez-Tejada, S.M. Alam, S.M. Dennison, F.H. Jaeger, K.
831 Anasti, S. Stewart, J.H. Blinn, H.X. Liao, J.G. Sodroski, B.F. Haynes, and S.J. Danishefsky.
832 2013. Chemical synthesis of highly congested gp120 V1V2 N-glycopeptide antigens for
833 potential HIV-1-directed vaccines. *J. Am. Chem. Soc.* 135:13113-13120.

834 Barouch, D.H., J.B. Whitney, B. Moldt, F. Klein, T.Y. Oliveira, J. Liu, K.E. Stephenson, H.W. Chang,
835 K. Shekhar, S. Gupta, J.P. Nkolola, M.S. Seaman, K.M. Smith, E.N. Borducchi, C. Cabral,
836 J.Y. Smith, S. Blackmore, S. Sanisetty, J.R. Perry, M. Beck, M.G. Lewis, W. Rinaldi, A.K.
837 Chakraborty, P. Poignard, M.C. Nussenzweig, and D.R. Burton. 2013. Therapeutic
838 efficacy of potent neutralizing HIV-1-specific monoclonal antibodies in SHIV-infected
839 rhesus monkeys. *Nature* 503:224-228.

840 Behrens, A.J., S. Vasiljevic, L.K. Pritchard, D.J. Harvey, R.S. Andev, S.A. Krumm, W.B. Struwe, A.
841 Cupo, A. Kumar, N. Zitzmann, G.E. Seabright, H.B. Kramer, D.I. Spencer, L. Royle, J.H.
842 Lee, P.J. Klasse, D.R. Burton, I.A. Wilson, A.B. Ward, R.W. Sanders, J.P. Moore, K.J.
843 Doores, and M. Crispin. 2016. Composition and antigenic effects of individual glycan
844 sites of a trimeric HIV-1 envelope glycoprotein. *Cell. Rep.* 14:2695-2706.

845 Bonsignori, M., K.K. Hwang, X. Chen, C.Y. Tsao, L. Morris, E. Gray, D.J. Marshall, J.A. Crump, S.H.
846 Kapiga, N.E. Sam, F. Sinangil, M. Pancera, Y. Yongping, B. Zhang, J. Zhu, P.D. Kwong, S.

847 O'Dell, J.R. Mascola, L. Wu, G.J. Nabel, S. Phogat, M.S. Seaman, J.F. Whitesides, M.A.
848 Moody, G. Kelsoe, X. Yang, J. Sodroski, G.M. Shaw, D.C. Montefiori, T.B. Kepler, G.D.
849 Tomaras, S.M. Alam, H.X. Liao, and B.F. Haynes. 2011. Analysis of a clonal lineage of
850 HIV-1 envelope V2/V3 conformational epitope-specific broadly neutralizing
851 antibodies and their inferred unmutated common ancestors. *J. Virol.* 85:9998-10009.

852 Bonsignori, M., H.X. Liao, F. Gao, W.B. Williams, S.M. Alam, D.C. Montefiori, and B.F. Haynes.
853 2017. Antibody-virus co-evolution in HIV infection: paths for HIV vaccine
854 development. *Immunol Rev* 275:145-160.

855 Burton, D.R., and J.R. Mascola. 2015. Antibody responses to envelope glycoproteins in HIV-1
856 infection. *Nat Immunol* 16:571-576.

857 Chen, L., Y.D. Kwon, T. Zhou, X. Wu, S. O'Dell, L. Cavacini, A.J. Hessell, M. Pancera, M. Tang, L.
858 Xu, Z.Y. Yang, M.Y. Zhang, J. Arthos, D.R. Burton, D.S. Dimitrov, G.J. Nabel, M.R. Posner, J.
859 Sodroski, R. Wyatt, J.R. Mascola, and P.D. Kwong. 2009. Structural basis of immune
860 evasion at the site of CD4 attachment on HIV-1 gp120. *Science* 326:1123-1127.

861 Chen, V.B., W.B. Arendall, 3rd, J.J. Headd, D.A. Keedy, R.M. Immormino, G.J. Kapral, L.W.
862 Murray, J.S. Richardson, and D.C. Richardson. 2010. MolProbity: all-atom structure
863 validation for macromolecular crystallography. *Acta Crystallogr D Biol Crystallogr.*
864 66:12-21.

865 Crespillo, S., S. Casares, P.L. Mateo, and F. Conejero-Lara. 2014. Thermodynamic analysis of the
866 binding of 2F5 (Fab and immunoglobulin G forms) to its gp41 epitope reveals a strong
867 influence of the immunoglobulin Fc region on affinity. *J Biol Chem* 289:594-599.

868 de Taeye, S.W., J.P. Moore, and R.W. Sanders. 2016. HIV-1 Envelope Trimer Design and
869 Immunization Strategies To Induce Broadly Neutralizing Antibodies. *Trends Immunol*
870 37:221-232.

871 de Taeye, S.W., G. Ozorowski, d.l.P. Torrents, M. Guttman, J.P. Julien, T.L. van den Kerkhof, J.A.
872 Burger, L.K. Pritchard, P. Pugach, A. Yasmeen, J. Crampton, J. Hu, I. Bontjer, J.L. Torres,
873 H. Arendt, J. DeStefano, W.C. Koff, H. Schuitemaker, D. Eggink, B. Berkhout, H. Dean, C.
874 LaBranche, S. Crotty, M. Crispin, D.C. Montefiori, P.J. Klasse, K.K. Lee, J.P. Moore, I.A.
875 Wilson, A.B. Ward, and R.W. Sanders. 2015. Immunogenicity of stabilized HIV-1
876 envelope trimers with reduced exposure of non-neutralizing epitopes. *Cell* 163:1702-
877 1715.

878 Derking, R., G. Ozorowski, K. Sliepen, A. Yasmeen, A. Cupo, J.L. Torres, J.P. Julien, J.H. Lee, T. van
879 Montfort, S.W. de Taeye, M. Connors, D.R. Burton, I.A. Wilson, P.J. Klasse, A.B. Ward, J.P.
880 Moore, and R.W. Sanders. 2015. Comprehensive antigenic map of a cleaved soluble
881 HIV-1 envelope trimer. *PLoS Pathog.* 11:e1004767.

882 Doria-Rose, N.A., C.A. Schramm, J. Gorman, P.L. Moore, J.N. Bhiman, B.J. DeKosky, M.J.
883 Ernandes, I.S. Georgiev, H.J. Kim, M. Pancera, R.P. Staupe, H.R. Altae-Tran, R.T. Bailer,
884 E.T. Crooks, A. Cupo, A. Druz, N.J. Garrett, K.H. Hoi, R. Kong, M.K. Louder, N.S. Longo, K.
885 McKee, M. Nonyane, S. O'Dell, R.S. Roark, R.S. Rudicell, S.D. Schmidt, D.J. Sheward, C.
886 Soto, C.K. Wibmer, Y. Yang, Z. Zhang, J.C. Mullikin, J.M. Binley, R.W. Sanders, I.A. Wilson,
887 J.P. Moore, A.B. Ward, G. Georgiou, C. Williamson, S.S. Abdool Karim, L. Morris, P.D.
888 Kwong, L. Shapiro, and J.R. Mascola. 2014. Developmental pathway for potent V1V2-
889 directed HIV-neutralizing antibodies. *Nature* 509:55-62.

Dosenovic, P., B.L. von, A. Escolano, J. Jardine, N.T. Freund, A.D. Gitlin, A.T. McGuire, D.W. Kulp, T. Oliveira, L. Scharf, J. Pietzsch, M.D. Gray, A. Cupo, M.J. van Gils, K.H. Yao, C. Liu, A. Gazumyan, M.S. Seaman, P.J. Bjorkman, R.W. Sanders, J.P. Moore, L. Stamatatos, W.R. Schief, and M.C. Nussenzweig. 2015. Immunization for HIV-1 broadly neutralizing antibodies in human Ig knockin mice. *Cell* 161:1505-1515.

Emsley, P., and K. Cowtan. 2004. Coot: model-building tools for molecular graphics. *Acta Crystallogr D Biol Crystallogr.* 60:2126-2132.

Escolano, A., P. Dosenovic, and M.C. Nussenzweig. 2017. Progress toward active or passive HIV-1 vaccination. *J Exp Med* 214:3-16.

Escolano, A., J.M. Steichen, P. Dosenovic, D.W. Kulp, J. Golijanin, D. Sok, N.T. Freund, A.D. Gitlin, T. Oliveira, T. Araki, S. Lowe, S.T. Chen, J. Heinemann, K.H. Yao, E. Georgeson, K.L. Saye-Francisco, A. Gazumyan, Y. Adachi, M. Kubitz, D.R. Burton, W.R. Schief, and M.C. Nussenzweig. 2016. Sequential immunization elicits broadly neutralizing anti-HIV-1 antibodies in Ig knockin mice. *Cell* 166:1445-1458 e1412.

Euler, Z., E.M. Bunnik, J.A. Burger, B.D. Boeser-Nunnink, M.L. Grijsen, J.M. Prins, and H. Schuitemaker. 2011. Activity of broadly neutralizing antibodies, including PG9, PG16, and VRC01, against recently transmitted subtype B HIV-1 variants from early and late in the epidemic. *J. Virol.* 85:7236-7245.

Euler, Z., M.J. van Gils, E.M. Bunnik, P. Phung, B. Schweighardt, T. Wrin, and H. Schuitemaker. 2010. Cross-reactive neutralizing humoral immunity does not protect from HIV type 1 disease progression. *J. Infect. Dis.* 201:1045-1053.

911 Fera, D., A.G. Schmidt, B.F. Haynes, F. Gao, H.X. Liao, T.B. Kepler, and S.C. Harrison. 2014.
912 Affinity maturation in an HIV broadly neutralizing B-cell lineage through reorientation
913 of variable domains. *Proc Natl Acad Sci U S A* 111:10275-10280.

914 Garces, F., J.H. Lee, V.N. de, A.T. de la Pena, L. Kong, C. Puchades, Y. Hua, R.L. Stanfield, D.R.
915 Burton, J.P. Moore, R.W. Sanders, A.B. Ward, and I.A. Wilson. 2015. Affinity maturation
916 of a potent family of HIV antibodies is primarily focused on accommodating or
917 avoiding glycans. *Immunity* 43:1053-1063.

918 Garces, F., D. Sok, L. Kong, R. McBride, H.J. Kim, K.F. Saye-Francisco, J.P. Julien, Y. Hua, A. Cupo,
919 J.P. Moore, J.C. Paulson, A.B. Ward, D.R. Burton, and I.A. Wilson. 2014. Structural
920 evolution of glycan recognition by a family of potent HIV antibodies. *Cell* 159:69-79.

921 Gautam, R., Y. Nishimura, A. Pegu, M.C. Nason, F. Klein, A. Gazumyan, J. Golijanin, A. Buckler-
922 White, R. Sadjadpour, K. Wang, Z. Mankoff, S.D. Schmidt, J.D. Lifson, J.R. Mascola, M.C.
923 Nussenzweig, and M.A. Martin. 2016. A single injection of anti-HIV-1 antibodies
924 protects against repeated SHIV challenges. *Nature* 533:105-109.

925 Gorman, J., C. Soto, M.M. Yang, T.M. Davenport, M. Guttman, R.T. Bailer, M. Chambers, G.Y.
926 Chuang, B.J. DeKosky, N.A. Doria-Rose, A. Druz, M.J. Ernandes, I.S. Georgiev, M.C.
927 Jarosinski, M.G. Joyce, T.M. Lemmin, S. Leung, M.K. Louder, J.R. McDaniel, S. Narpala, M.
928 Pancera, J. Stuckey, X. Wu, Y. Yang, B. Zhang, T. Zhou, N.C. Program, J.C. Mullikin, U.
929 Baxa, G. Georgiou, A.B. McDermott, M. Bonsignori, B.F. Haynes, P.L. Moore, L. Morris,
930 K.K. Lee, L. Shapiro, J.R. Mascola, and P.D. Kwong. 2016. Structures of HIV-1 Env V1V2
931 with broadly neutralizing antibodies reveal commonalities that enable vaccine design.
932 *Nat. Struct. Mol. Biol.* 23:81-90.

933 Gristick, H.B., L. von Boehmer, A.P. West, Jr., M. Schamber, A. Gazumyan, J. Golijanin, M.S.
934 Seaman, G. Fatkenheuer, F. Klein, M.C. Nussenzweig, and P.J. Bjorkman. 2016. Natively
935 glycosylated HIV-1 Env structure reveals new mode for antibody recognition of the
936 CD4-binding site. *Nat Struct Mol Biol* 23:906-915.

937 Haynes, B.F., G. Kelsoe, S.C. Harrison, and T.B. Kepler. 2012. B-cell-lineage immunogen design
938 in vaccine development with HIV-1 as a case study. *Nat. Biotechnol.* 30:423-433.

939 Hessell, A.J., P. Poignard, M. Hunter, L. Hangartner, D.M. Tehrani, W.K. Bleeker, P.W. Parren,
940 P.A. Marx, and D.R. Burton. 2009. Effective, low-titer antibody protection against low-
941 dose repeated mucosal SHIV challenge in macaques. *Nat. Med.* 15:951-954.

942 Hraber, P., M.S. Seaman, R.T. Bailer, J.R. Mascola, D.C. Montefiori, and B.T. Korber. 2014.
943 Prevalence of broadly neutralizing antibody responses during chronic HIV-1 infection.
944 *AIDS* 28:163-169.

945 Jardine, J., J.P. Julien, S. Menis, T. Ota, O. Kalyuzhniy, A. McGuire, D. Sok, P.S. Huang, S.
946 MacPherson, M. Jones, T. Nieusma, J. Mathison, D. Baker, A.B. Ward, D.R. Burton, L.
947 Stamatatos, D. Nemazee, I.A. Wilson, and W.R. Schief. 2013. Rational HIV immunogen
948 design to target specific germline B cell receptors. *Science* 340:711-716.

949 Jardine, J.G., D.W. Kulp, C. Havenar-Daughton, A. Sarkar, B. Briney, D. Sok, F. Sesterhenn, J.
950 Ereno-Orbea, O. Kalyuzhniy, I. Deresa, X. Hu, S. Spencer, M. Jones, E. Georgeson, Y.
951 Adachi, M. Kubitz, A.C. deCamp, J.P. Julien, I.A. Wilson, D.R. Burton, S. Crotty, and W.R.
952 Schief. 2016. HIV-1 broadly neutralizing antibody precursor B cells revealed by
953 germline-targeting immunogen. *Science* 351:1458-1463.

954 Jardine, J.G., T. Ota, D. Sok, M. Pauthner, D.W. Kulp, O. Kalyuzhniy, P.D. Skog, T.C. Thinnes, D.
955 Bhullar, B. Briney, S. Menis, M. Jones, M. Kubitz, S. Spencer, Y. Adachi, D.R. Burton, W.R.
956 Schief, and D. Nemazee. 2015. Priming a broadly neutralizing antibody response to
957 HIV-1 using a germline-targeting immunogen. *Science* 349:156-161.

958 Joyce, M.G., M. Kanekiyo, L. Xu, C. Biertumpfel, J.C. Boyington, S. Moquin, W. Shi, X. Wu, Y. Yang,
959 Z.Y. Yang, B. Zhang, A. Zheng, T. Zhou, J. Zhu, J.R. Mascola, P.D. Kwong, and G.J. Nabel.
960 2013. Outer domain of HIV-1 gp120: antigenic optimization, structural malleability,
961 and crystal structure with antibody VRC-PG04. *J. Virol.* 87:2294-2306.

962 Julien, J.P., A. Cupo, D. Sok, R.L. Stanfield, D. Lyumkis, M.C. Deller, P.J. Klasse, D.R. Burton, R.W.
963 Sanders, J.P. Moore, A.B. Ward, and I.A. Wilson. 2013. Crystal structure of a soluble
964 cleaved HIV-1 envelope trimer. *Science* 342:1477-1483.

965 Karlsson, R., J.A. Mo, and R. Holmdahl. 1995. Binding of autoreactive mouse anti-type II
966 collagen antibodies derived from the primary and the secondary immune response
967 investigated with the biosensor technique. *J Immunol Methods* 188:63-71.

968 Klasse, P.J., C.C. LaBranche, T.J. Ketas, G. Ozorowski, A. Cupo, P. Pugach, R.P. Ringe, M. Golabek,
969 M.J. van Gils, M. Guttman, K.K. Lee, I.A. Wilson, S.T. Butera, A.B. Ward, D.C. Montefiori,
970 R.W. Sanders, and J.P. Moore. 2016. Sequential and Simultaneous Immunization of
971 Rabbits with HIV-1 Envelope Glycoprotein SOSIP.664 Trimers from Clades A, B and C.
972 *PLoS Pathog* 12:e1005864.

973 Klein, F., R. Diskin, J.F. Scheid, C. Gaebler, H. Mouquet, I.S. Georgiev, M. Pancera, T. Zhou, R.B.
974 Incesu, B.Z. Fu, P.N. Gnanapragasam, T.Y. Oliveira, M.S. Seaman, P.D. Kwong, P.J.
975 Bjorkman, and M.C. Nussenzweig. 2013a. Somatic mutations of the immunoglobulin

framework are generally required for broad and potent HIV-1 neutralization. *Cell* 153:126-138.

Klein, F., H. Mouquet, P. Dosenovic, J.F. Scheid, L. Scharf, and M.C. Nussenzweig. 2013b. Antibodies in HIV-1 vaccine development and therapy. *Science* 341:1199-1204.

Klein, J.S., and P.J. Bjorkman. 2010. Few and far between: how HIV may be evading antibody avidity. *PLoS Pathog* 6:e1000908.

Kong, L., B. Ju, Y. Chen, L. He, L. Ren, J. Liu, K. Hong, B. Su, Z. Wang, G. Ozorowski, X. Ji, Y. Hua, Y. Chen, M.C. Deller, Y. Hao, Y. Feng, F. Garces, R. Wilson, K. Dai, S. O'Dell, K. McKee, J.R. Mascola, A.B. Ward, R.T. Wyatt, Y. Li, I.A. Wilson, J. Zhu, and Y. Shao. 2016. Key gp120 glycans pose roadblocks to the rapid development of VRC01-class antibodies in an HIV-1-infected chinese donor. *Immunity* 44:939-950.

Labrijn, A.F., P. Poignard, A. Raja, M.B. Zwick, K. Delgado, M. Franti, J. Binley, V. Vivona, C. Grundner, C.C. Huang, M. Venturi, C.J. Petropoulos, T. Wrin, D.S. Dimitrov, J. Robinson, P.D. Kwong, R.T. Wyatt, J. Sodroski, and D.R. Burton. 2003. Access of antibody molecules to the conserved coreceptor binding site on glycoprotein gp120 is sterically restricted on primary human immunodeficiency virus type 1. *J Virol* 77:10557-10565.

Li, Y., S. O'Dell, L.M. Walker, X. Wu, J. Guenaga, Y. Feng, S.D. Schmidt, K. McKee, M.K. Louder, J.E. Ledgerwood, B.S. Graham, B.F. Haynes, D.R. Burton, R.T. Wyatt, and J.R. Mascola. 2011. Mechanism of neutralization by the broadly neutralizing HIV-1 monoclonal antibody VRC01. *J. Virol.* 85:8954-8967.

Liao, H.X., R. Lynch, T. Zhou, F. Gao, S.M. Alam, S.D. Boyd, A.Z. Fire, K.M. Roskin, C.A. Schramm, Z. Zhang, J. Zhu, L. Shapiro, J.C. Mullikin, S. Gnanakaran, P. Hraber, K. Wiehe, G. Kelsoe,

998 G. Yang, S.M. Xia, D.C. Montefiori, R. Parks, K.E. Lloyd, R.M. Scearce, K.A. Soderberg, M.
999 Cohen, G. Kamanga, M.K. Louder, L.M. Tran, Y. Chen, F. Cai, S. Chen, S. Moquin, X. Du,
1000 M.G. Joyce, S. Srivatsan, B. Zhang, A. Zheng, G.M. Shaw, B.H. Hahn, T.B. Kepler, B.T.
1001 Korber, P.D. Kwong, J.R. Mascola, and B.F. Haynes. 2013. Co-evolution of a broadly
1002 neutralizing HIV-1 antibody and founder virus. *Nature* 496:469-476.

1003 Lynch, R.M., P. Wong, L. Tran, S. O'Dell, M.C. Nason, Y. Li, X. Wu, and J.R. Mascola. 2015. HIV-1
1004 fitness cost associated with escape from the VRC01 class of CD4 binding site
1005 neutralizing antibodies. *J. Virol.* 89:4201-4213.

1006 Mascola, J.R., and B.F. Haynes. 2013. HIV-1 neutralizing antibodies: understanding nature's
1007 pathways. *Immunol. Rev.* 254:225-244.

1008 McGuire, A.T., M.D. Gray, P. Dosenovic, A.D. Gitlin, N.T. Freund, J. Petersen, C. Correnti, W.
1009 Johnsen, R. Kegel, A.B. Stuart, J. Glenn, M.S. Seaman, W.R. Schief, R.K. Strong, M.C.
1010 Nussenzweig, and L. Stamatatos. 2016. Specifically modified Env immunogens activate
1011 B-cell precursors of broadly neutralizing HIV-1 antibodies in transgenic mice. *Nat.*
1012 *Commun.* 7:10618.

1013 McGuire, A.T., S. Hoot, A.M. Dreyer, A. Lippy, A. Stuart, K.W. Cohen, J. Jardine, S. Menis, J.F.
1014 Scheid, A.P. West, W.R. Schief, and L. Stamatatos. 2013. Engineering HIV envelope
1015 protein to activate germline B cell receptors of broadly neutralizing anti-CD4 binding
1016 site antibodies. *J. Exp. Med.* 210:655-663.

1017 McLellan, J.S., M. Pancera, C. Carrico, J. Gorman, J.P. Julien, R. Khayat, R. Louder, R. Pejchal, M.
1018 Sastry, K. Dai, S. O'Dell, N. Patel, S. Shahzad-ul-Hussan, Y. Yang, B. Zhang, T. Zhou, J.
1019 Zhu, J.C. Boyington, G.Y. Chuang, D. Diwanji, I. Georgiev, Y.D. Kwon, D. Lee, M.K. Louder,
1020 S. Moquin, S.D. Schmidt, Z.Y. Yang, M. Bonsignori, J.A. Crump, S.H. Kapiga, N.E. Sam, B.F.

Haynes, D.R. Burton, W.C. Koff, L.M. Walker, S. Phogat, R. Wyatt, J. Orwenyo, L.X. Wang, J. Arthos, C.A. Bewley, J.R. Mascola, G.J. Nabel, W.R. Schief, A.B. Ward, I.A. Wilson, and P.D. Kwong. 2011. Structure of HIV-1 gp120 V1/V2 domain with broadly neutralizing antibody PG9. *Nature* 480:336-343.

Medina-Ramirez, M., R.W. Sanders, and Q.J. Sattentau. 2017. Stabilized HIV-1 envelope glycoprotein trimers for vaccine use. *Curr Opin HIV AIDS*

Mouquet, H., J.F. Scheid, M.J. Zoller, M. Krogsgaard, R.G. Ott, S. Shukair, M.N. Artyomov, J. Pietzsch, M. Connors, F. Pereyra, B.D. Walker, D.D. Ho, P.C. Wilson, M.S. Seaman, H.N. Eisen, A.K. Chakraborty, T.J. Hope, J.V. Ravetch, H. Wardemann, and M.C. Nussenzweig. 2010. Polyreactivity increases the apparent affinity of anti-HIV antibodies by heteroligation. *Nature* 467:591-595.

Neilson, J.R., G.C. John, J.K. Carr, P. Lewis, J.K. Kreiss, S. Jackson, R.W. Nduati, D. Mbori-Ngacha, D.D. Panteleeff, S. Bodrug, C. Giachetti, M.A. Bott, B.A. Richardson, J. Bwayo, J. Ndinya-Achola, and J. Overbaugh. 1999. Subtypes of human immunodeficiency virus type 1 and disease stage among women in Nairobi, Kenya. *J. Virol.* 73:4393-4403.

Ota, T., C. Doyle-Cooper, A.B. Cooper, M. Huber, E. Falkowska, K.J. Doores, L. Hangartner, K. Le, D. Sok, J. Jardine, J. Lifson, X. Wu, J.R. Mascola, P. Poignard, J.M. Binley, B.K. Chakrabarti, W.R. Schief, R.T. Wyatt, D.R. Burton, and D. Nemazee. 2012. Anti-HIV B Cell lines as candidate vaccine biosensors. *J. Immunol.* 189:4816-4824.

Otwinowski, Z., and W. Minor. 1997. Processing of X-ray diffraction data collected in oscillation mode. *Methods. Enzymol.* 276:307–326.

1042 Pancera, M., J.S. McLellan, X. Wu, J. Zhu, A. Changela, S.D. Schmidt, Y. Yang, T. Zhou, S. Phogat,
1043 J.R. Mascola, and P.D. Kwong. 2010. Crystal structure of PG16 and chimeric dissection
1044 with somatically related PG9: structure-function analysis of two quaternary-specific
1045 antibodies that effectively neutralize HIV-1. *J. Virol.* 84:8098-8110.

1046 Pancera, M., T. Zhou, A. Druz, I.S. Georgiev, C. Soto, J. Gorman, J. Huang, P. Acharya, G.Y. Chuang,
1047 G. Ofek, G.B. Stewart-Jones, J. Stuckey, R.T. Bailer, M.G. Joyce, M.K. Louder, N. Tumba, Y.
1048 Yang, B. Zhang, M.S. Cohen, B.F. Haynes, J.R. Mascola, L. Morris, J.B. Munro, S.C.
1049 Blanchard, W. Mothes, M. Connors, and P.D. Kwong. 2014. Structure and immune
1050 recognition of trimeric pre-fusion HIV-1 Env. *Nature* 514:455-461.

1051 Peden, K., M. Emerman, and L. Montagnier. 1991. Changes in growth properties on passage in
1052 tissue culture of viruses derived from infectious molecular clones of HIV-1LAI, HIV-
1053 1MAL, and HIV-1ELI. *Virology* 185:661-672.

1054 Pelanda, R., S. Schwers, E. Sonoda, R.M. Torres, D. Nemazee, and K. Rajewsky. 1997. Receptor
1055 editing in a transgenic mouse model: site, efficiency, and role in B cell tolerance and
1056 antibody diversification. *Immunity* 7:765-775.

1057 Pritchard, L.K., S. Vasiljevic, G. Ozorowski, G.E. Seabright, A. Cupo, R. Ringe, H.J. Kim, R.W.
1058 Sanders, K.J. Doores, D.R. Burton, I.A. Wilson, A.B. Ward, J.P. Moore, and M. Crispin.
1059 2015. Structural constraints determine the glycosylation of HIV-1 envelope trimers.
1060 *Cell Rep.* 11:1604-1613.

1061 Pugach, P., G. Ozorowski, A. Cupo, R. Ringe, A. Yasmeen, V.N. de, R. Derking, H.J. Kim, J. Korzun,
1062 M. Golabek, R.K. de Los, T.J. Ketas, J.P. Julien, D.R. Burton, I.A. Wilson, R.W. Sanders, P.J.
1063 Klasse, A.B. Ward, and J.P. Moore. 2015. A native-like SOSIP.664 trimer based on an
1064 HIV-1 subtype B env gene. *J. Virol.* 89:3380-3395.

1065 Sanders, R.W., R. Derking, A. Cupo, J.P. Julien, A. Yasmeen, V.N. de, H.J. Kim, C. Blattner, A.T. de
1066 la Pena, J. Korzun, M. Golabek, R.K. de Los, T.J. Ketas, M.J. van Gils, C.R. King, I.A. Wilson,
1067 A.B. Ward, P.J. Klasse, and J.P. Moore. 2013. A next-generation cleaved, soluble HIV-1
1068 Env trimer, BG505 SOSIP.664 gp140, expresses multiple epitopes for broadly
1069 neutralizing but not non-neutralizing antibodies. *PLoS Pathog.* 9:e1003618.

1070 Sanders, R.W., and J.P. Moore. 2017. Native-like Env trimers as a platform for HIV-1 vaccine
1071 design. *Immunol Rev* 275:161-182.

1072 Sanders, R.W., A.E. van, A.A. Nabatov, I.M. Liscaljet, I. Bontjer, D. Eggink, M. Melchers, E. Busser,
1073 M.M. Dankers, F. Groot, I. Braakman, B. Berkhout, and W.A. Paxton. 2008. The
1074 carbohydrate at asparagine 386 on HIV-1 gp120 is not essential for protein folding
1075 and function but is involved in immune evasion. *Retrovirology* 5:10.

1076 Sanders, R.W., M.J. van Gils, R. Derking, D. Sok, T.J. Ketas, J.A. Burger, G. Ozorowski, A. Cupo, C.
1077 Simonich, L. Goo, H. Arendt, H.J. Kim, J.H. Lee, P. Pugach, M. Williams, G. Debnath, B.
1078 Moldt, M.J. van Breemen, G. Isik, M. Medina-Ramirez, J.W. Back, W.C. Koff, J.P. Julien,
1079 E.G. Rakasz, M.S. Seaman, M. Guttman, K.K. Lee, P.J. Klasse, C. LaBranche, W.R. Schief,
1080 I.A. Wilson, J. Overbaugh, D.R. Burton, A.B. Ward, D.C. Montefiori, H. Dean, and J.P.
1081 Moore. 2015. HIV-1 neutralizing antibodies induced by native-like envelope trimers.
1082 *Science* 349:aac4223.

1083 Saphire, E.O., R.L. Stanfield, M.D. Crispin, P.W. Parren, P.M. Rudd, R.A. Dwek, D.R. Burton, and
1084 I.A. Wilson. 2002. Contrasting IgG structures reveal extreme asymmetry and flexibility.
1085 *J Mol Biol* 319:9-18.

1086 Scharf, L., A.P. West, Jr., H. Gao, T. Lee, J.F. Scheid, M.C. Nussenzweig, P.J. Bjorkman, and R.
1087 Diskin. 2013. Structural basis for HIV-1 gp120 recognition by a germ-line version of a
1088 broadly neutralizing antibody. *Proc Natl Acad Sci U S A* 110:6049-6054.

1089 Scharf, L., A.P. West, S.A. Sievers, C. Chen, S. Jiang, H. Gao, M.D. Gray, A.T. McGuire, J.F. Scheid,
1090 M.C. Nussenzweig, L. Stamatatos, and P.J. Bjorkman. 2016. Structural basis for
1091 germline antibody recognition of HIV-1 immunogens. *eLife* 5, e13783:

1092 Scheid, J.F., H. Mouquet, N. Feldhahn, M.S. Seaman, K. Velinzon, J. Pietzsch, R.G. Ott, R.M.
1093 Anthony, H. Zebroski, A. Hurley, A. Phogat, B. Chakrabarti, Y. Li, M. Connors, F. Pereyra,
1094 B.D. Walker, H. Wardemann, D. Ho, R.T. Wyatt, J.R. Mascola, J.V. Ravetch, and M.C.
1095 Nussenzweig. 2009. Broad diversity of neutralizing antibodies isolated from memory
1096 B cells in HIV-infected individuals. *Nature* 458:636-640.

1097 Scheid, J.F., H. Mouquet, B. Ueberheide, R. Diskin, F. Klein, T.Y. Oliveira, J. Pietzsch, D. Fenyo, A.
1098 Abadir, K. Velinzon, A. Hurley, S. Myung, F. Boulad, P. Poignard, D.R. Burton, F. Pereyra,
1099 D.D. Ho, B.D. Walker, M.S. Seaman, P.J. Bjorkman, B.T. Chait, and M.C. Nussenzweig.
1100 2011. Sequence and structural convergence of broad and potent HIV antibodies that
1101 mimic CD4 binding. *Science* 333:1633-1637.

1102 Shih, T.A., M. Roederer, and M.C. Nussenzweig. 2002. Role of antigen receptor affinity in T cell-
1103 independent antibody responses in vivo. *Nat. Immunol.* 3:399-406.

1104 Shingai, M., O.K. Donau, R.J. Plishka, A. Buckler-White, J.R. Mascola, G.J. Nabel, M.C. Nason, D.
1105 Montefiori, B. Moldt, P. Poignard, R. Diskin, P.J. Bjorkman, M.A. Eckhaus, F. Klein, H.
1106 Mouquet, J.C. Cetrulo Lorenzi, A. Gazumyan, D.R. Burton, M.C. Nussenzweig, M.A.
1107 Martin, and Y. Nishimura. 2014. Passive transfer of modest titers of potent and

broadly neutralizing anti-HIV monoclonal antibodies block SHIV infection in macaques. *J. Exp. Med.* 211:2061-2074.

Sliepen, K., M. Medina-Ramirez, A. Yasmeen, J.P. Moore, P.J. Klasse, and R.W. Sanders. 2015. Binding of inferred germline precursors of broadly neutralizing HIV-1 antibodies to native-like envelope trimers. *Virology* 486:116-120.

Sok, D., B. Briney, J.G. Jardine, D.W. Kulp, S. Menis, M. Pauthner, A. Wood, E.C. Lee, K.M. Le, M. Jones, A. Ramos, O. Kalyuzhniy, Y. Adachi, M. Kubitz, S. MacPherson, A. Bradley, G.A. Friedrich, W.R. Schief, and D.R. Burton. 2016. Priming HIV-1 broadly neutralizing antibody precursors in human Ig loci transgenic mice. *Science* 353:1557-1560.

Sok, D., M.J. van Gils, M. Pauthner, J.P. Julien, K.L. Saye-Francisco, J. Hsueh, B. Briney, J.H. Lee, K.M. Le, P.S. Lee, Y. Hua, M.S. Seaman, J.P. Moore, A.B. Ward, I.A. Wilson, R.W. Sanders, and D.R. Burton. 2014. Recombinant HIV envelope trimer selects for quaternary-dependent antibodies targeting the trimer apex. *PNAS* 111:17624-17629.

Stamatatos, L., M. Pancera, and A.T. McGuire. 2017. Germline-targeting immunogens. *Immunol Rev* 275:203-216.

Steichen, J.M., D.W. Kulp, T. Tokatlian, A. Escolano, P. Dosenovic, R.L. Stanfield, L.E. McCoy, G. Ozorowski, X. Hu, O. Kalyuzhniy, B. Briney, T. Schiffner, F. Garces, N.T. Freund, A.D. Gitlin, S. Menis, E. Georgeson, M. Kubitz, Y. Adachi, M. Jones, A.A. Mutafyan, D.S. Yun, C.T. Mayer, A.B. Ward, D.R. Burton, I.A. Wilson, D.J. Irvine, M.C. Nussenzweig, and W.R. Schief. 2016. HIV vaccine design to target germline precursors of glycan-dependent broadly neutralizing antibodies. *Immunity* 45:483-496.

1129 Tian, M., C. Cheng, X. Chen, H. Duan, H.L. Cheng, M. Dao, Z. Sheng, M. Kimble, L. Wang, S. Lin,
1130 S.D. Schmidt, Z. Du, M.G. Joyce, Y. Chen, B.J. DeKosky, Y. Chen, E. Normandin, E. Cantor,
1131 R.E. Chen, N.A. Doria-Rose, Y. Zhang, W. Shi, W.P. Kong, M. Choe, A.R. Henry, F.
1132 Laboune, I.S. Georgiev, P.Y. Huang, S. Jain, A.T. McGuire, E. Georgeson, S. Menis, D.C.
1133 Douek, W.R. Schief, L. Stamatatos, P.D. Kwong, L. Shapiro, B.F. Haynes, J.R. Mascola, and
1134 F.W. Alt. 2016. Induction of HIV Neutralizing Antibody Lineages in Mice with Diverse
1135 Precursor Repertoires. *Cell* 166:1471-1484 e1418.

1136 van den Kerkhof, T.L., K.A. Feenstra, Z. Euler, M.J. van Gils, L.W. Rijsdijk, B.D. Boeser-Nunnink,
1137 J. Heringa, H. Schuitemaker, and R.W. Sanders. 2013. HIV-1 envelope glycoprotein
1138 signatures that correlate with the development of cross-reactive neutralizing activity.
1139 *Retrovirology* 10:102.

1140 van Gils, M.J., and R.W. Sanders. 2013. Broadly neutralizing antibodies against HIV-1:
1141 templates for a vaccine. *Virology* 435:46-56.

1142 Verkoczy, L., F.W. Alt, and M. Tian. 2017. Human Ig knockin mice to study the development
1143 and regulation of HIV-1 broadly neutralizing antibodies. *Immunol Rev* 275:89-107.

1144 Walker, L.M., M. Huber, K.J. Doores, E. Falkowska, R. Pejchal, J.P. Julien, S.K. Wang, A. Ramos,
1145 P.Y. Chan-Hui, M. Moyle, J.L. Mitcham, P.W. Hammond, O.A. Olsen, P. Phung, S. Fling,
1146 C.H. Wong, S. Phogat, T. Wrin, M.D. Simek, W.C. Koff, I.A. Wilson, D.R. Burton, and P.
1147 Poignard. 2011. Broad neutralization coverage of HIV by multiple highly potent
1148 antibodies. *Nature* 477:466-470.

1149 Walker, L.M., S.K. Phogat, P.Y. Chan-Hui, D. Wagner, P. Phung, J.L. Goss, T. Wrin, M.D. Simek, S.
1150 Fling, J.L. Mitcham, J.K. Lehrman, F.H. Priddy, O.A. Olsen, S.M. Frey, P.W. Hammond, S.
1151 Kaminsky, T. Zamb, M. Moyle, W.C. Koff, P. Poignard, and D.R. Burton. 2009. Broad and

potent neutralizing antibodies from an African donor reveal a new HIV-1 vaccine target. *Science* 326:285-289.

Ward, A.B., and I.A. Wilson. 2017. The HIV-1 envelope glycoprotein structure: nailing down a moving target. *Immunol Rev* 275:21-32.

Weiss, M.S., and R. Hilgenfeld. 1997. On the use of the merging R factor as a quality indicator for X-ray data. *J. Appl. Crystallog.* 30:203-205.

West, A.P., Jr., R. Diskin, M.C. Nussenzweig, and P.J. Bjorkman. 2012. Structural basis for germ-line gene usage of a potent class of antibodies targeting the CD4-binding site of HIV-1 gp120. *PNAS* 109:E2083-E2090.

Woods, A.S., H.Y. Wang, and S.N. Jackson. 2007. Sulfation, the up-and-coming post-translational modification: its role and mechanism in protein-protein interaction. *J. Proteome. Res.* 6:1176-1182.

Wu, X., A.B. Parast, B.A. Richardson, R. Nduati, G. John-Stewart, D. Mbori-Ngacha, S.M. Rainwater, and J. Overbaugh. 2006. Neutralization escape variants of human immunodeficiency virus type 1 are transmitted from mother to infant. *J. Virol.* 80:835-844.

Wu, X., T. Zhou, J. Zhu, B. Zhang, I. Georgiev, C. Wang, X. Chen, N.S. Longo, M. Louder, K. McKee, S. O'Dell, S. Perfetto, S.D. Schmidt, W. Shi, L. Wu, Y. Yang, Z.Y. Yang, Z. Yang, Z. Zhang, M. Bonsignori, J.A. Crump, S.H. Kapiga, N.E. Sam, B.F. Haynes, M. Simek, D.R. Burton, W.C. Koff, N.A. Doria-Rose, M. Connors, N.C.S. Program, J.C. Mullikin, G.J. Nabel, M. Roederer, L. Shapiro, P.D. Kwong, and J.R. Mascola. 2011. Focused evolution of HIV-1 neutralizing antibodies revealed by structures and deep sequencing. *Science* 333:1593-1602.

1174 Xiao, X., W. Chen, Y. Feng, and D.S. Dimitrov. 2009a. Maturation pathways of cross-reactive
1175 HIV-1 neutralizing antibodies. *Viruses* 1:802-817.

1176 Xiao, X., W. Chen, Y. Feng, Z. Zhu, P. Prabakaran, Y. Wang, M.Y. Zhang, N.S. Longo, and D.S.
1177 Dimitrov. 2009b. Germline-like predecessors of broadly neutralizing antibodies lack
1178 measurable binding to HIV-1 envelope glycoproteins: implications for evasion of
1179 immune responses and design of vaccine immunogens. *Biochem. Biophys. Res.*
1180 *Commun.* 390:404-409.

1181 Yasmeen, A., R. Ringe, R. Derking, A. Cupo, J.P. Julien, D.R. Burton, A.B. Ward, I.A. Wilson, R.W.
1182 Sanders, J.P. Moore, and P.J. Klasse. 2014. Differential binding of neutralizing and non-
1183 neutralizing antibodies to native-like soluble HIV-1 Env trimers, uncleaved Env
1184 proteins, and monomeric subunits. *Retrovirology* 11:41.

1185 Zhou, T., I. Georgiev, X. Wu, Z.Y. Yang, K. Dai, A. Finzi, Y.D. Kwon, J.F. Scheid, W. Shi, L. Xu, Y.
1186 Yang, J. Zhu, M.C. Nussenzweig, J. Sodroski, L. Shapiro, G.J. Nabel, J.R. Mascola, and P.D.
1187 Kwong. 2010. Structural basis for broad and potent neutralization of HIV-1 by
1188 antibody VRC01. *Science* 329:811-817.

1189 Zhou, T., J. Zhu, X. Wu, S. Moquin, B. Zhang, P. Acharya, I.S. Georgiev, H.R. Altae-Tran, G.Y.
1190 Chuang, M.G. Joyce, Y.D. Kwon, N.S. Longo, M.K. Louder, T. Luongo, K. McKee, C.A.
1191 Schramm, J. Skinner, Y. Yang, Z. Yang, Z. Zhang, A. Zheng, M. Bonsignori, B.F. Haynes,
1192 J.F. Scheid, M.C. Nussenzweig, M. Simek, D.R. Burton, W.C. Koff, N.C.S. Program, J.C.
1193 Mullikin, M. Connors, L. Shapiro, G.J. Nabel, J.R. Mascola, and P.D. Kwong. 2013.
1194 Multidonor analysis reveals structural elements, genetic determinants, and
1195 maturation pathway for HIV-1 neutralization by VRC01-class antibodies. *Immunity*
1196 39:245-258.

## Figures legends

**Figure 1**. **Design and biophysical properties of a germline-targeting SOSIP trimer.** (**A**) Schematic of the BG505 SOSIP.v.4.1-GT1 construct (also referred to as GT1 trimer). The constant (C1 to C5) and variable (V1 to V5) regions in gp120 and the HR1 and HR2 regions in gp41 are indicated. The SOSIP mutations as well as the added N332 PNGS are shown in red. The E64K and A316W stabilizing mutations introduced to the SOSIP.664 construct to create SOSIP.v4.1 are indicated in blue. The mutations then introduced to SOSIP.v4.1 to induce gl-bNAb binding are indicated in green. The approximate position of a 7 amino-acid deletion is indicated with magenta arrows and a white dashed line. The glycan composition is adapted from Behrens et al. (2015). (**B**) Overview of the 18 changes introduced to BG505 SOSIP.664 to obtain SOSIP.v4.1-GT1. (**C**) NS-EM analyses of the GT1 trimer purified by PGT145. The 2D class averages are shown. Based on loop-movement, compactness and angles between individual protomers, the trimers are classified as closed native-like, partially open native-like, or non-native (Pugach et al., 2015). The proportion of each class is indicated. (**D**) DSC analysis of the GT1 trimer purified with PGT145. The $T_m$ value is indicated. (**E**) Glycan profiles of PGT145-purified trimer variants as determined by HILIC-UPLC. The percentages of $Man_{5\text{-}9}GlcNAc_2$ glycans (M5-M9; shown in green), as a proportion of the total glycan population, are listed in **Table S6**.

**Figure 2**. **Antigenicity of the BG505 SOSIP.v4.1-GT1 trimer with a panel of bNAbs and gl-bNAbs.** (**A**) Binding of bNAbs and gl-bNAbs to different SOSIP trimers was assessed by capture ELISA. Half maximal binding concentrations ($EC_{50}$, in μg/ml) are shown and ranges in ng/ml are color-coded. (**B**) Representative binding SPR curves of the binding of PG16 and VRC01 mature and germline versions to SOSIP.v4.1 and SOSIP.v4.1-GT1. The sensorgrams show the response (RU) over time (seconds). The association phase is 300s and the dissociation is followed over 600s. Curves for concentration ranges (see inset) are shown in color with the modeled fits in black overlaid with the corresponding dissociation constant ($K_d = K_{d1}$ for the monovalent initial interaction, see **Table S7**). SPR experiments were performed at least 3 times independently.

**Figure 3**. **Overall architecture of BG505 SOSIP.v4.1-GT1-N137A at 3.2 Å.** (**A**) Left, side view of the trimer in complex with 9H+109L and 35O22 Fabs. The three protomers of the trimer complex are depicted as a surface representation (front left), spheres (back) and ribbon (front right) the latter with gp41 (in cyan) and gp120 (in blue). Each Env protomer (blue) is associated with one Fab 9H+109L (brown) and one Fab 35O22 (yellow). Glycans are shown in red sticks. Right, structural alignment of one protomer (ribbon) from BG505 SOSIP.v4.1-GT1-N137A at 3.2 Å (gp120 in blue and gp41 in cyan) superimposed on one protomer of BG505 SOSIP.664-N137A (gray, PDB 5CEZ). The root mean square deviation is indicated and *N*-linked glycans are shown and numbered by their respective Asn residues. (**B**) Ribbon representation of one protomer illustrating the mutations introduced to SOSIP.v4.1-GT1 to improve

stability and enhance gl-bNAb-binding. (**C**) Zoomed in 180° views of the apex region. Mutations are indicated with arrows and the side chains are represented as sticks. The asterisk indicates the location of the truncated V2 loop after the 7-amino acid deletion. (**D**) Detailed view of the V3 showing the A316W substitution with a 2Fo-Fc electron density map contoured at 1.0σ.

**Figure 4. Structural mechanism of germline engagement.** (**A**) Model of the interaction between PG9 HCDR3 (red) and V1V2 epitope of BG505 SOSIP.v4.1-GT1-N137A (blue). Relevant amino-acid positions are indicated and side chains are shown as blue sticks for Env and red sticks for HCDR3. Predicted interactions (<4 Å) between side chains are indicated with black dashed lines. (**B**) Model of interaction between the light chain of gl-VRC01 (green) and the loop D of SOSIP.v4.1-GT1-N137A (blue). Predicted interactions (<4 Å) between side chains are indicated with black dashed lines. The D462 residue, a substitution made to delete a possible obstructing glycan, is shown in the background (surface red). An intra-protomer H-bond (<4 Å) between T455 and S471 is indicated with black dashed lines. (**C**) Interaction between gl-VRC01 and the CD4bs, modeled in two different views. The positions of three PNGS in BG505 are indicated with spheres and their likely clashes with gl-VRCO1 light chain by red explosion shapes.

**Figure 5**. **BG505 SOSIP.v4.1-GT1 initiates antibody responses in knock-in mice expressing the predicted germlines of VRC01 and PGT121 bNAbs.** (**A**) Calcium flux in B cells expressing either gl-VRC01 (left) or VRC01 (right) as a B-cell receptor,

stimulated with the indicated trimers at a 1 μM final concentration. In this and the subsequent panels, all of the trimers used as immunogens and ELISA antigens were of the BG505 genotype. (**B**) Endpoint antibody binding titers in sera from $gl_H$-VRC01 mice immunized thrice with either SOSIP.v4.1-GT1 (left), SOSIP.v4.1 (center) or SOSIP.664 (right) trimers, measured against the indicated His-tagged BG505 trimer variants by ELISA. The median titers are indicated by the black line. Statistically significant differences are indicated by asterisks (*, P≤0.05; **, P≤0.01; Wilcoxon matched-pairs signed rank test). The ELISA curves can be found in **Fig. S5A**. (**C**) Antibody specificity determinations. For each mouse, the area under the curve (Fig. S8) for a given gl-VRC01 epitope knock-out trimer (SOSIP.v4.1-D368R or SOSIP.v4.1-GT1-D368R) was subtracted from the area under the curve obtained with the corresponding unmodified trimer (i.e. SOSIP.v4.1 or SOSIP.v4.1-GT1). The resulting "area above knock-out (KO)" values are plotted as bars. The ELISA curves used for the area under the curve analyses can be found in **Fig S5A**. The method has been described before . The mean and standard error of the mean (SEM) are indicated. Statistically significant differences are indicated by asterisks (*, P≤0.05; Wilcoxon matched-pairs signed rank test). (**D**) Endpoint antibody binding titers in sera from $gl_H$-PGT121 mice immunized thrice with either SOSIP.v4.1-GT1 (left) or SOSIP.v4.1 (right) trimers, measured against the indicated His-tagged BG505 trimer variants by ELISA. The median titers are indicated by the black line. Statistically significant differences are indicated by asterisks (*, P≤0.05; Wilcoxon matched-pairs signed rank test). The ELISA curves can be found in **Fig. S5B**. (**E**) Antibody specificity determinations. For each mouse, the area under the curve for the PGT121 epitope

knock-out trimer (SOSIP.v4.1-GT1-N137A/N332A/N301A/H330A) was subtracted from the area under the curve obtained with the unmodified trimer (i.e. SOSIP.v4.1-GT1). The resulting "area above knock-out (KO)" values are plotted as bars. The ELISA curves used for the area under the curve analyses can be found in **Fig S5B**. The mean and standard error of the mean (SEM) are indicated. Statistically significant differences are indicated by asterisks (*, P≤0.05; Wilcoxon matched-pairs signed rank test).

**Figure S1**. **Related to Figure 2A and 5B-E. Antigenicity of BG505 SOSIP.v4.1 and SOSIP.v4.1-GT1 trimers and analyses of epitope knock-out trimer mutants by ELISA.** The representative ELISA binding curves were derived using a panel of (**A**) mature bNAbs and (**B**) gl-bNAbs. The dilution factor for all antibodies was 1:3 except for gl-CH103 for which the dilution factor used was 1:2. (**C**) Binding of 2G12 (left), VRC01 (middle), and gl-VRC01 (right) to the trimer variants used for the analyses in Fig. 5. The overlapping 2G12 titration curves indicate that equivalent amounts of the various trimers (3.5ug/mL) were captured onto the ELISA wells. Binding of the mature VRC01 bNAb was reduced ~10 fold when the D368R substitution was introduced into the SOSIP.v4.1 trimer, but was not affected when the same D368R substitution was made in the SOSIP.v4.1-GT1 context. A possible explanation is that the loss of the antibody-trimer contact caused by the D368R change is compensated by other substitutions in and around the CD4bs of the GT1 trimer that are not present in SOSIP.v4.1. The gl-VRCO1 bNAb precursor did not bind the SOSIP.v4.1 trimer, but did bind the engineered GT1 variant. However, gl-VRC01 binding was no longer detectable when the D368R change was introduced into the GT1 construct. The gl-VRC01 antibody also bound the SOSIP.v4.1-N276D/T278R/Δ7 trimer mutant that lacked the N276 glycan and 7 amino acids in V2, albeit less well than the GT1 trimer. (B) Binding of 2G12 (left), PGT121 (middle), and gl-PGT121 (right) to the SOSIP.v4.1-GT1 trimer and the SOSIP.v4.1-GT1-N137A/N332A/N301A/H330A PGT121 epitope knock-out mutant. Although the four substitutions cause a partial reduction in 2G12 reactivity, PGT121 binding to the GT1 trimer is completely eliminated. The gl-PGT121 precursor does not bind to either the GT1 trimer or the quadruple mutant.

**Figure S2. Related to Figure 2B and Table S7**. **SPR analysis of binding of a panel of 6 bNAbs and their corresponding germline versions to three versions of BG505 SOSIP trimers.** The antibodies tested bind to a variety of epitopes (apex, CD4bs, N332/V3). The sensorgrams show the response (RU) over time (s). The association phase was 300s and dissociation was followed over 900s. Curves for concentration ranges (see inset) are shown in color.

**Figure S3. Related to Figure 2B. Antibody binding to Env trimers. SPR analysis of the binding of gl-VRC01, b6 and F105 to three versions of BG505 SOSIP trimers.** The sensorgrams show the response (RU) over time (s). The association phase was 300s and dissociation was followed over 900s. The colored curves show the responses obtained at a concentration of 500nM of each antibody.

**Figure S4. Related to Figures 3 and 4. Analysis of the 3H+109L and 9H+109L epitopes on the BG505 Env trimer and comparison of signature VRC01-class contacts in gl-bNAb Env complexes. (A)**

Superimposition of the crystal structure of Fab 9H+109L-BG505 SOSIP.v4.1-GT1-N137A complex with the Fab 3H+109L-BG505 SOSIP.664-N137A complex. The antibodies (putative heavy-chain precursors of the PGT121 family) and Env trimer are depicted as colored tubes while the glycans are shown as ball-and-sticks. **(B)** Expanded view of the 3H+109L and 9H+109L epitopes. The V1 region is highlighted by coloring Ala137 in yellow, and the GDIR motif in the V3 region is in red. Heavy chain (HC) (**C**) and light chain (LC) (**D and E**) contacts of gl-NIH45-46 with 426c.TM1ΔV1-3 (PDB code 5IGX) and gl-VRC01 with eOD-GT6 (PDB code 4JPK) superimposed onto the structure of BG505 SOSIP.v4.1-GT1-N137A. Protein backbones are shown as Cα traces, key interacting residues are shown in stick representations (red, oxygen; blue, nitrogen), and yellow dashed lines indicate putative hydrogen bonds (distance < 4 Å). Antibody: orange, gl-NIH45-46 HC; magenta, gl-NIH45-46 LC; yellow, gl-VRC01 HC; green, gl-VRC01 LC. gp120: blue, BG505 SOSIP.v4.1-GT1; light blue, 426c.TM1ΔV1-3. Panels A and C are based on similar figures in Scharf et al., 2016.

**Figure S5. Related to Figure 5B-E. Env trimer binding of sera derived from immunization of $gl_H$-VRC01 and $gl_H$-PGT121 knock-in mice with different SOSIP trimers.** (**A**) Sera (post-immunization 3) from $gl_H$-VRC01 knock-in mice immunized with BG505 SOSIP.v4.1-GT1 (left), SOSIP.v4.1 (middle) or SOSIP.664 (right) trimers were titrated against the indicated trimers by ELISA. The sera were serially diluted in three-fold steps, starting from a 1:100 dilution. (**B**) Sera (post-immunization 3) from $gl_H$-PGT121 knock-in mice immunized with BG505 SOSIP.v4.1-GT1 (left and middle) or SOSIP.v4.1 (right) trimers were titrated against the indicated trimers by ELISA. The sera were serially diluted in three-fold steps, starting from a 1:100 dilution.

**Figure S5. (continued)**

**Table S1**. **Related to Figs. 2, 5A, F (left panel), S3B and S7 and Tables S3-S5. Heavy and light chain sequences of the gl-bNAbs used in this study.**

**Table S2. Related to Figure 1A, B. Neutralization sensitivity of a panel of viruses to the inferred germline versions of PG9, PG16 and PGT145.** The TZM-bl cell assay was used to determine the percentage of neutralization at the maximum concentration of antibody. The ACS viruses are clinical isolates, BL035 and Q23 are Env-pseudotyped viruses and BG505 is a molecular clone (see SI Methods). The neutralization assays were performed in triplicate. The mean values, with standard deviations, are shown and ranged by color as indicated. The V2 sequence column shows the relevant sequences of residues 156 to 196 (HxB2 numbering system). The BG505 SOSIP.v4.1-GT1 sequence is indicated by the black arrow, the changes are highlighted in dark grey boxes/white characters, and the 7 amino-acid deletion is indicated by the gray shading over the dashed line. The origins of those changes are indicated by dashed boxes. The R178K change that was taken from elsewhere (Aussedat et al., 2013) is indicated with a shade of gray.

**Table S3. Related to Figure 1B. Relative binding of a panel of three gl-bNAbs and two bNAbs to BG505 SOSIP.664 variants in a D7324-capture ELISA using supernatants from transfected HEK293T cells**.

**Table S4. Related to Figure 1B. Relative binding of panel of three gl-bNAbs and two bNAbs to BG505 SOSIP.664 variants in a Ni-NTA/His-tag capture ELISA using supernatants from transfected HEK293T cells**.

**Table S5. Related to Figure 1B. Relative binding of panel of three gl-bNAbs and two bNAbs to BG505 SOSIP.664 variants by Ni-NTA/His-tag capture ELISA using affinity chromatography purified trimers.**

**Table S6. Related to Figure 1E. Percentage of $Man_{5-9}GlcNAc_2$ glycans (M5-M9) as the proportion of the total glycan population.**

**Table S7. Related to Figure 2B. SPR analysis of the mature and germline versions of a panel of bNAbs to SOSIP.664 trimer variants.**

**Table S8. Related to Figs. 3 and 4. X-ray data collection and refinement statistics.**

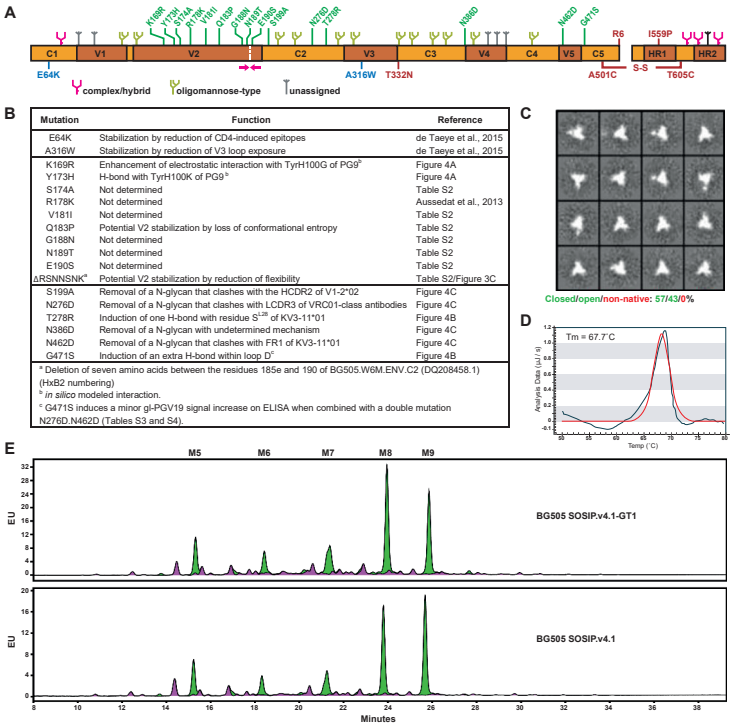


| Mutation | Function | Reference |
|---|---|---|
| E64K | Stabilization by reduction of CD4-induced epitopes | de Taeye et al., 2015 |
| A316W | Stabilization by reduction of V3 loop exposure | de Taeye et al., 2015 |
| K169R | Enhancement of electrostatic interaction with TyrH100G of PG9[c] | Figure 4A |
| Y173H | H-bond with TyrH100K of PG9[b] | Figure 4A |
| S174A | Not determined | Table S2 |
| R178K | Not determined | Aussedat et al., 2013 |
| V181I | Not determined | Table S2 |
| Q183P | Potential V2 stabilization by loss of conformational entropy | Table S2 |
| G188N | Not determined | Table S2 |
| N189T | Not determined | Table S2 |
| E190S | Not determined | Table S2 |
| ΔRSNNSNK[a] | Potential V2 stabilization by reduction of flexibility | Table S2/Figure 3C |
| S199A | Removal of a N-glycan that clashes with the HCDR2 of V1-2*02 | Figure 4C |
| N276D | Removal of a N-glycan that clashes with LCDR3 of VRC01-class antibodies | Figure 4C |
| T278R | Induction of one H-bond with residue $S^{L28}$ of KV3-11*01 | Figure 4B |
| N386D | Removal of a N-glycan with undetermined mechanism | Figure 4C |
| N462D | Removal of a N-glycan that clashes with FR1 of KV3-11*01 | Figure 4C |
| G471S | Induction of an extra H-bond within loop $D^{c}$ | Figure 4B |

[a] Deletion of seven amino acids between the residues 185e and 190 of BG505.W6M.ENV.C2 (DQ208458.1) (HxB2 numbering)
[b] *in silico* modeled interaction.
[c] G471S induces a minor gI-PGV19 signal increase on ELISA when combined with a double mutation N276D.N462D (Tables S3 and S4).

**A**

| Antigen | Mature antibodies | | | | | | | | | | | | | | | | Germline antibodies | | | | | | | | | |
|---|---|---|---|---|---|---|---|---|---|---|---|---|---|---|---|---|---|---|---|---|---|---|---|---|---|---|
| | Trimer apex | | | | | V3 glycan | | | | | CD4bs | | | | gp120/41 | | Trimer apex | | | CD4bs | | | | | gp41 | |
| | PG9 | PG16 | PGT145 | VRC26.09 | CH01 | 2G12 | PGT121 | PGT128 | PGT130 | PGT135 | VRC01 | 3BNC60 | 1NC9 | CH103 | PGT151 | 35O22 | PG9 | PG16 | CH01 | VRC01 | PGV19 | NIH45-46 | 12A12 | CH103 | 3BC315 | |
| BG505 SOSIP.v4.1 | 20 | 30 | 9 | 10 | 37 | 10 | 80 | 90 | 20 | 10 | 20 | 10 | 10 | 40 | 20 | 190 | 90 | 46 | 30 | >50000 | >50000 | >50000 | >50000 | 43000 | 45 | |
| BG505 SOSIP.v4.1-GT1 | 10 | 20 | 8 | 10 | 9 | 10 | 80 | 100 | 20 | 10 | 20 | 10 | 10 | 10 | 30 | 37 | 37 | 20 | 6 | 26 | 10 | 10 | 7000 | 35000 | 45 | |

EC50 (ng/ml)
<40
40-250
250-2500
2500-50000
>50000

**B**

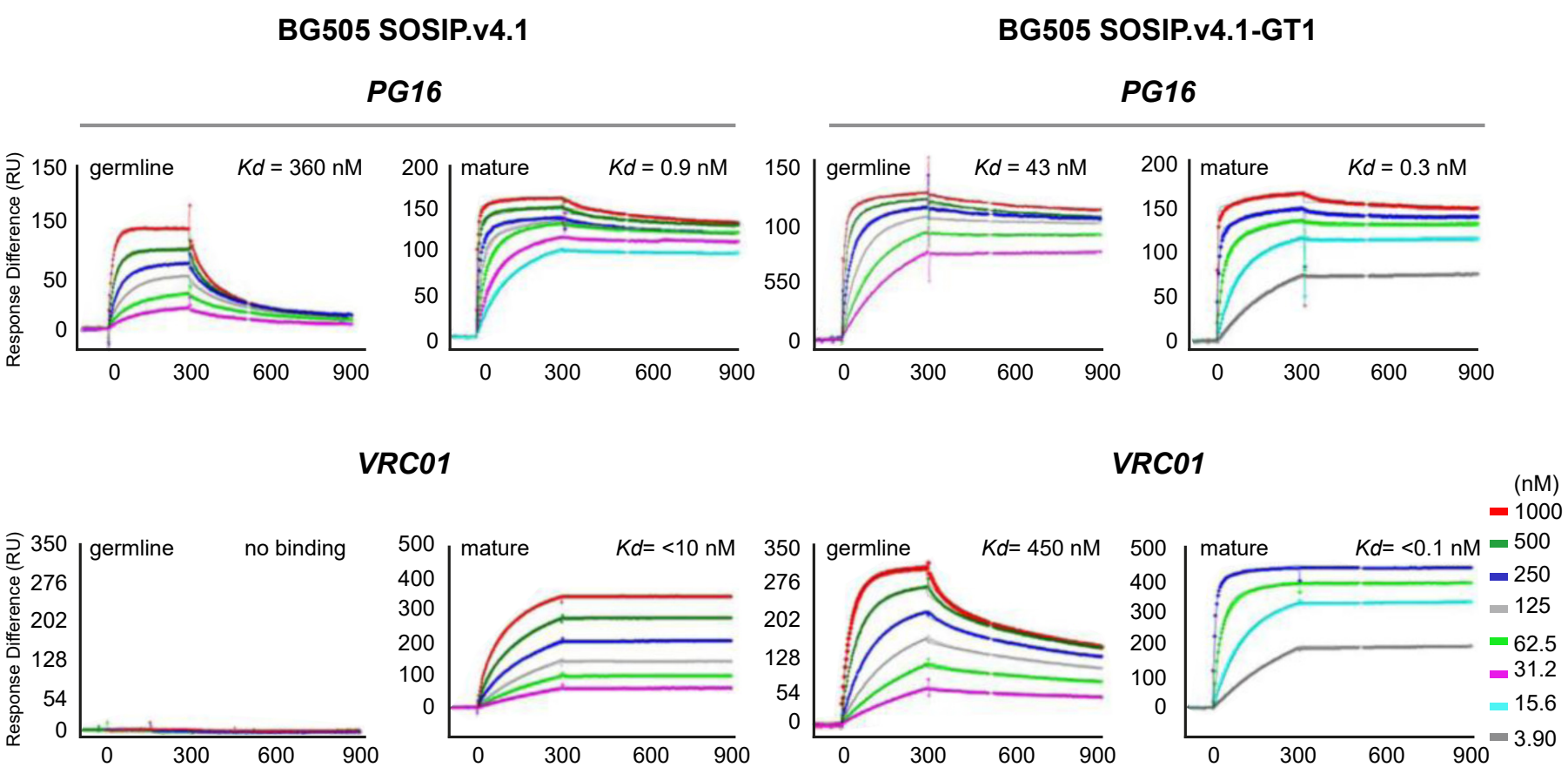

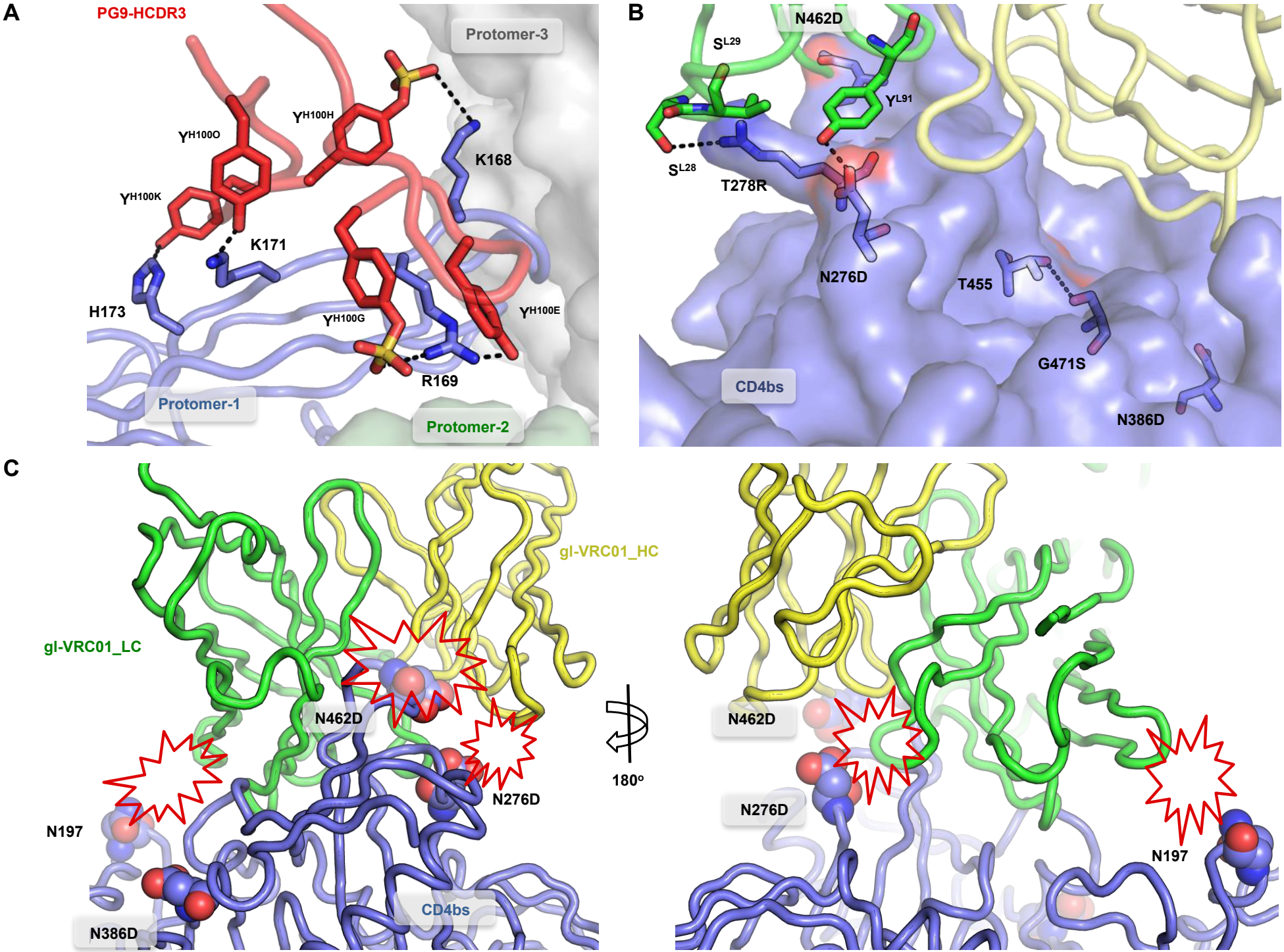
A
PG9-HCDR3
Protomer-3
YH100H
YH100O
K168
YH100K
K171
H173
YH100G
YH100E
R169
Protomer-1
Protomer-2
B
N462D
SL29
YL91
SL28
T278R
N276D
T455
G471S
CD4bs
N386D
C
gl-VRC01_HC
gl-VRC01_LC
N462D
N276D
N197
CD4bs
N386D
180°
N462D
N276D
N197

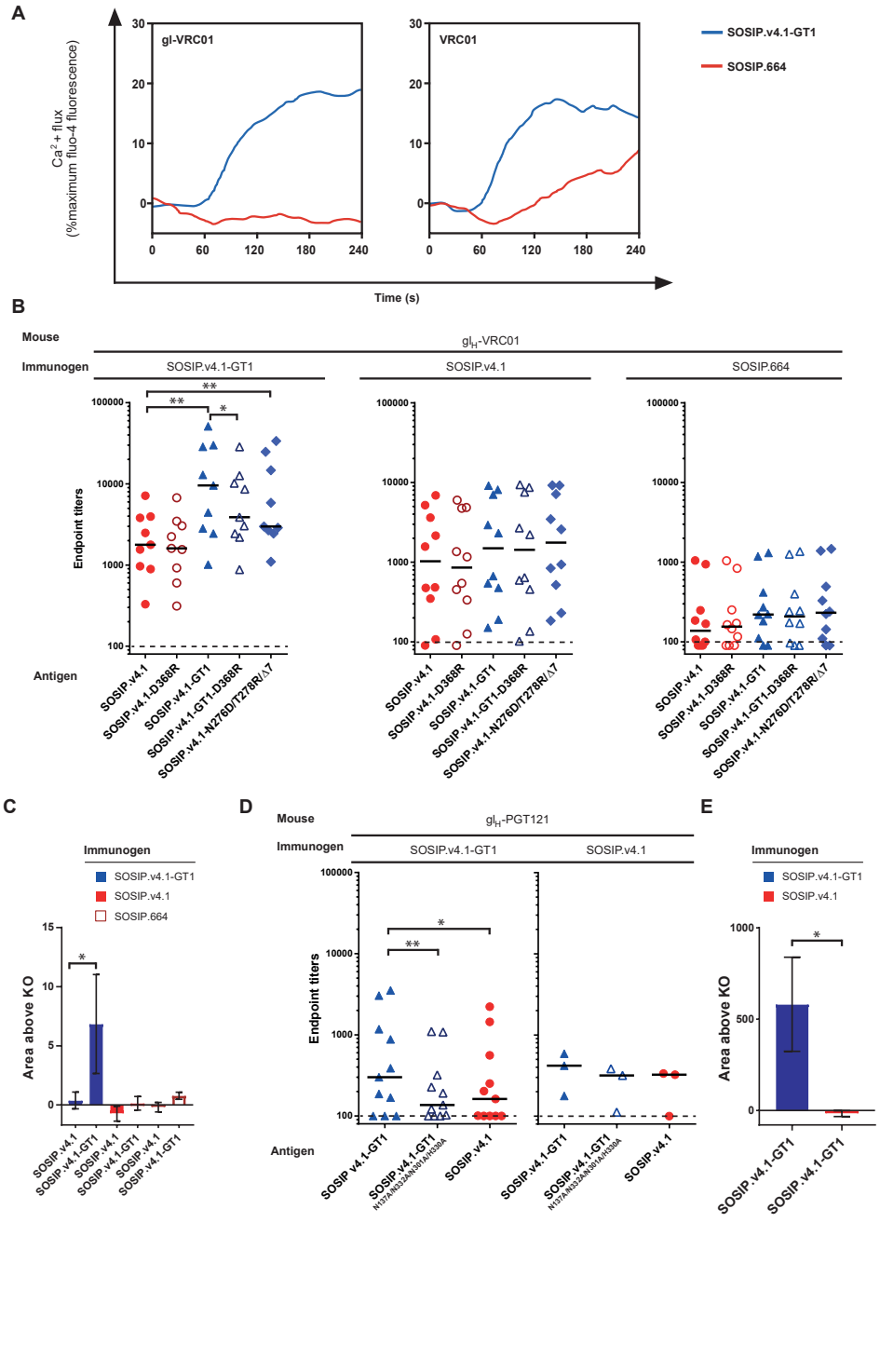
A
gl-VRC01
VRC01
SOSIP.v4.1-GT1
SOSIP.664
Ca2+ flux
(%maximum fluo-4 fluorescence)
Time (s)
B
Mouse
glH-VRC01
Immunogen
SOSIP.v4.1-GT1
SOSIP.v4.1
SOSIP.664
Endpoint titers
Antigen
SOSIP.v4.1
SOSIP.v4.1-D368R
SOSIP.v4.1-GT1
SOSIP.v4.1-GT1-D368R
SOSIP.v4.1-N276D/T278R/ΔT
C
Immunogen
SOSIP.v4.1-GT1
SOSIP.v4.1
SOSIP.664
Area above KO
D
Mouse
glH-PGT121
Immunogen
SOSIP.v4.1-GT1
SOSIP.v4.1
Endpoint titers
Antigen
SOSIP.v4.1-GT1
SOSIP.v4.1-GT1 N137A/N332A/N301H/S308A
SOSIP.v4.1
E
Immunogen
SOSIP.v4.1-GT1
SOSIP.v4.1
Area above KO

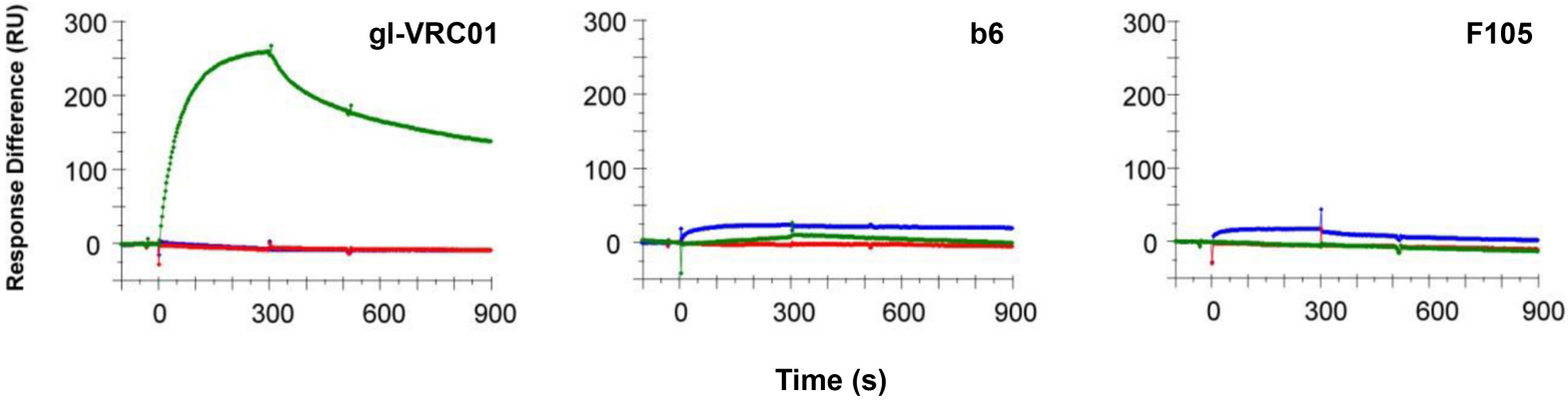


BG505 SOSIP.664

BG505 SOSIP.v4.1

BG505 SOSIP.v4.1-GT1

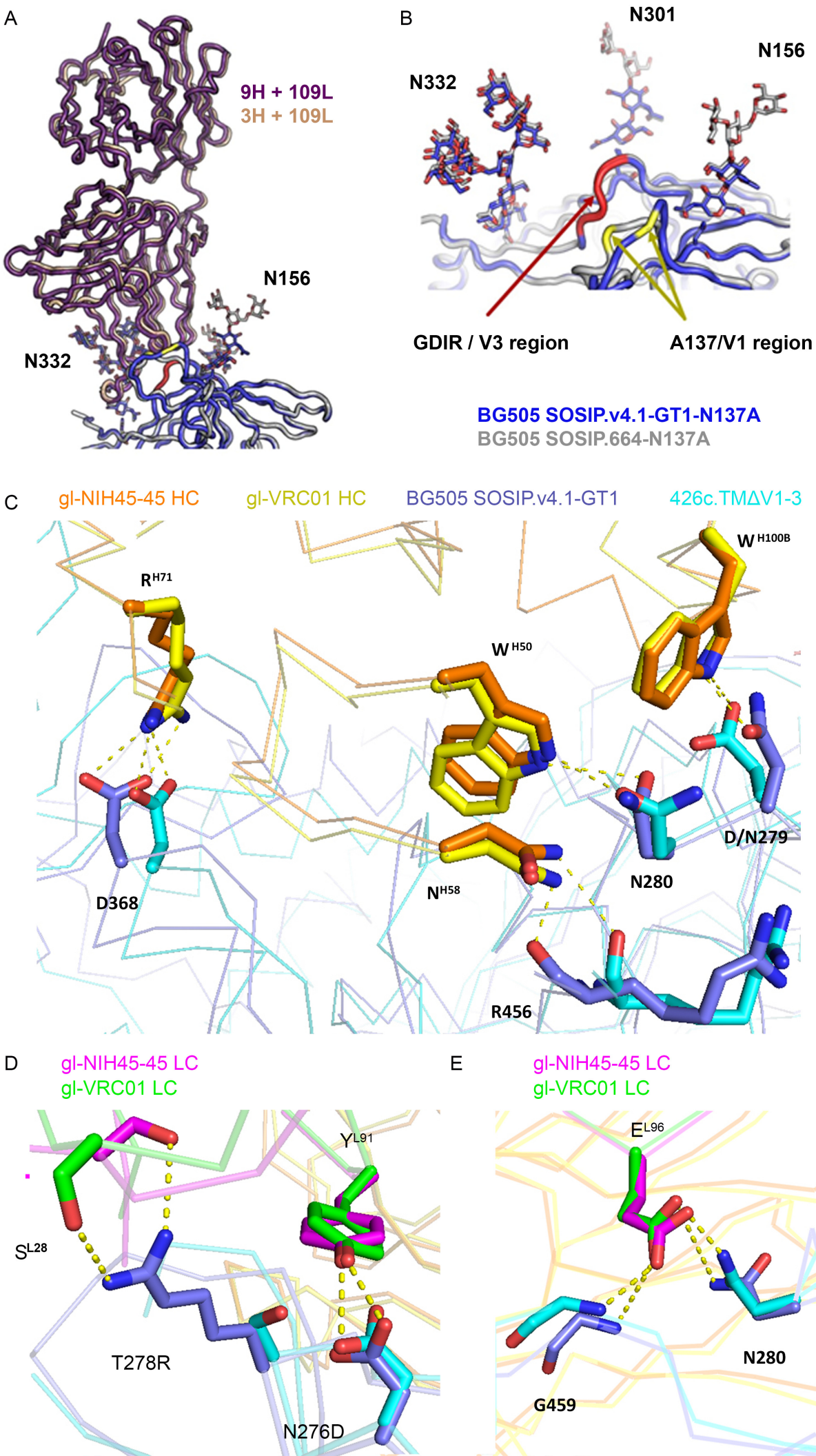
A
9H + 109L
3H + 109L
N156
N332
B
N301
N156
N332
GDIR / V3 region
A137/V1 region
BG505 SOSIP.v4.1-GT1-N137A
BG505 SOSIP.664-N137A
C
gl-NIH45-45 HC
gl-VRC01 HC
BG505 SOSIP.v4.1-GT1
426c.TMΔV1-3
R H71
W H50
W H100B
D368
N H58
D/N279
N280
R456
D
gl-NIH45-45 LC
gl-VRC01 LC
Y L91
S L28
T278R
N276D
E
gl-NIH45-45 LC
gl-VRC01 LC
E L96
N280
G459

gl-$_H$VRC01

**Immunogen**

| BG505 SOSIP.v4.1-GT1 | BG505 SOSIP.v4.1 | BG505 SOSIP.664 |
|---|---|---|
| Mouse 3016 | Mouse 3001 | Mouse 3049 |
| Mouse 3015 | Mouse 3002 | Mouse 3050 |
| Mouse 3017 | Mouse 3010 | Mouse 3051 |
| Mouse 3018 | Mouse 3011 | Mouse 3052 |
| Mouse 3019 | Mouse 3012 | Mouse 3053 |
| Mouse 3303 | Mouse 3013 | Mouse 3054 |
| Mouse 3304 | Mouse 3014 | Mouse 3055 |
| Mouse 3305 | Mouse 4998 | Mouse 3056 |
| Mouse 3306 | Mouse 4999 | Mouse 3057 |
| | Mouse 5000 | Mouse 3058 |

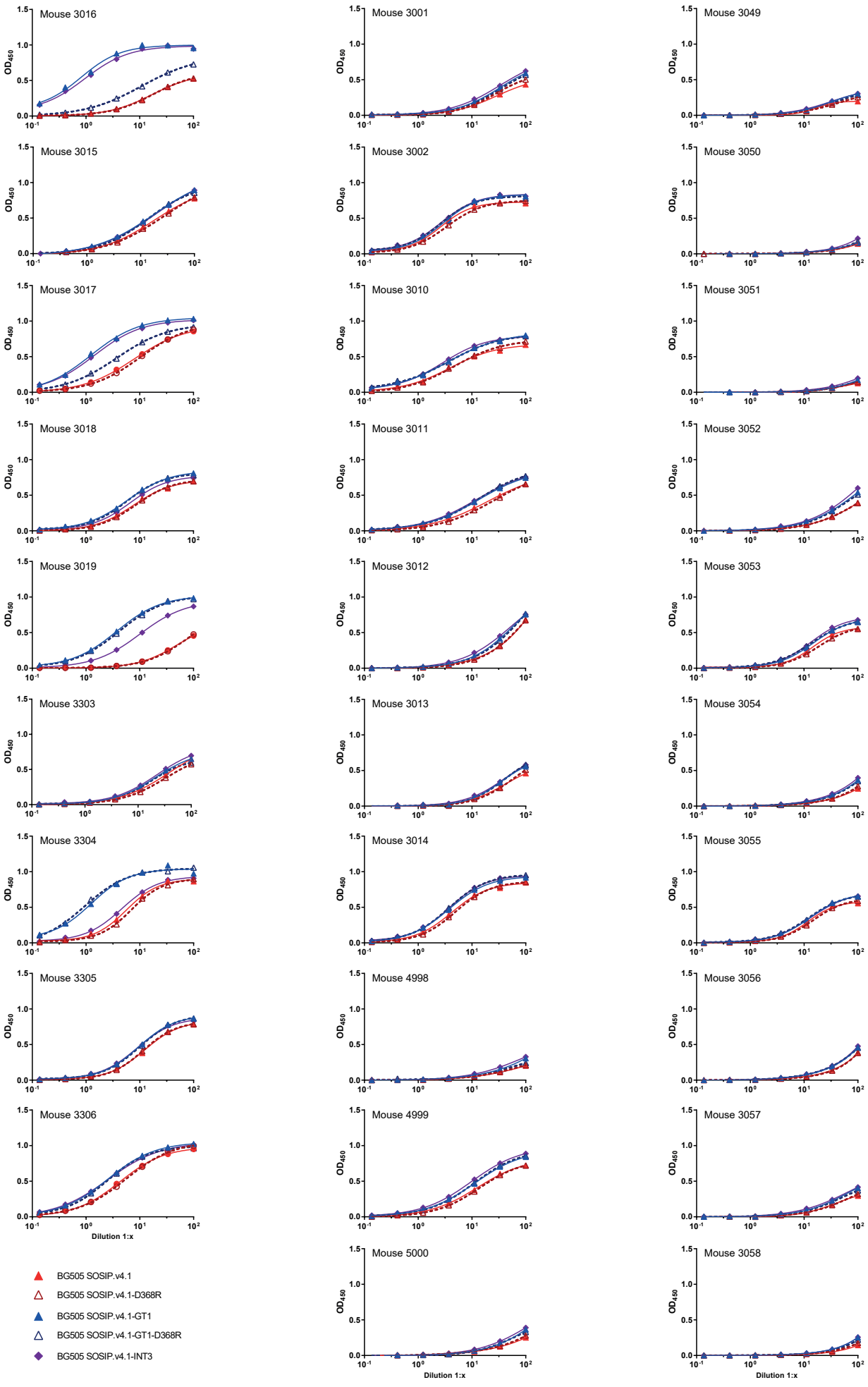

gl-$_H$PGT121

**Immunogen**

BG505 SOSIP.v4.1-GT1

BG505 SOSIP.v4.1

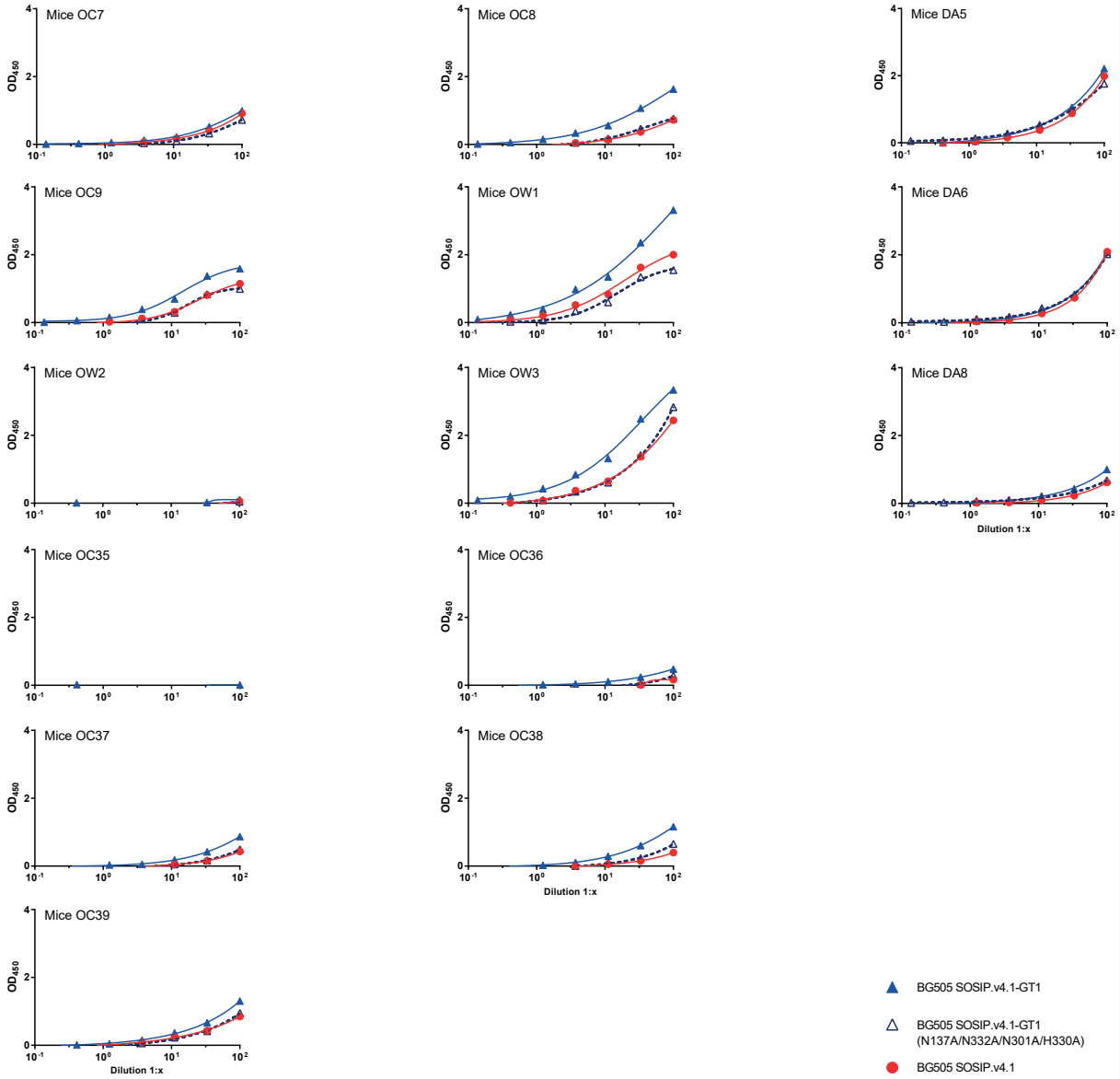

# Supplemental Tables

**Table S1. Related to Figs. 2, 5A, F (left panel), S3B and S7 and Tables S3-S5. Heavy and light chain sequences of the gl-bNAbs used in this study.**

| | | |
|---|---|---|
| PG9[1] | VH reverted | QVQLVESGGGVVQPGRSLRLSCAASGFTFSSYGMHWVRQAPGKGLEWVAVISYDGSNKYYADSVKGRFTISRDNSKNTLYLQMNSLRAEDTAVYYCAREAGGPDYRNGYNYYDFWSGYYTYYYMDVWGKGTTVTVSS |
| | VL reverted | QSALTQPASVSGSPGQSITISCTGTSSDVGGYNYVSWYQQHPGKAPKLMIYEVSNRPSGVSNRFSGSKSGNTASLTISGLQAEDEADYYCSSYTSSSTLVFGGGTKLTVL |
| PG16[2] | VH reverted | QVQLVESGGGVVQPGRSLRLSCAASGFTFSSYGMHWVRQAPGKGLEWVAVISYDGSNKYYADSVKGRFTISRDNSKNTLYLQMNSLRAEDTAVYYCAREAGGPIWHDDVKYYDFNDGYYNYHYMDVWGKGTTVTVSS |
| | VL reverted | QSALTQPASVSGSPGQSITISCTGTSSDVGGYNYVSWYQQHPGKAPKLMIYEVSNRPSGVSNRFSGSKSGNTASLTISGLQAEDEADYYCSSYTSSSTLIFGGGTKVTVL |
| PG145[1] | VH reverted | QVQLVQSGAEVKKPGASVKVSCKASGYTFTSYDINWVRQATGQGLEWMGWMNPNSGNTGYAQKFQGRVTMTRNTSISTAYMELSSLRSEDTAVYYCARGSKHRLRDYFLYNEYGPNYEEWGDYLATLDVWGQGTMVTVSS |
| | VL reverted | DIVMTQSPLSLPVTPGEPASISCRSSQSLLHSNGYNYLDWYLQKPGQSPQLLIYLGSNRASGVPDRFSGSGSGTDFTLKISRVEAEDVGVYYCMQALQTPWTFGQGTKVEIK |
| CH01[3] | VH reverted | EVQLVESGGGVVRPGGSLRLSCAASGFTFDDYGMSWVRQAPGKGLEWVSGINWNGGSTGYADSVKGRFTISRDNAKNSLYLQMNSLRAEDTALYYCARGTDYTIDDQGIRYQGSGTFWYFDLWGRGTLVTVSS |
| | VL reverted | EIVLTQSPGTLSLSPGERATLSCRASQSVSSSYLAWYQQKPGQAPRLLIYGASSRATGIPDRFSGSGSGTDFTLTISRLEPEDFAVYYCQQYGSSPYTFGQGTKVEIK |
| PGT121[4] | VH reverted* | QVQLQESGPGLVKPSETLSLTCTVSGGSISSYYWSWIRQPPGKGLEWIGYIYYSGSTNYNPSLKSRVTISVDTSKNQFSLKLSSVTAADTAVYYCARTQQGKRIYGVVSFGDYYYYYYMDVWGKGTTVTVSS |
| | VL reverted | SYVLTQPPSVSVAPGQTARITCGGNNIGSKSVHWYQQKPGQAPVLVVYDDSDRPSGIPERFSGSNSGNTATLTISRVEAGDEADYYCQVWDSSSDHPWVFGGGTKLTVL |
| 1NC9[1] | VH reverted | QVQLVQSGAEVKKPGASVKVSCKASGYTFTSYYMHWVRQAPGQGLEWMGIINPSGGSTSYAQKFQGRVTMTRDTSTSTVYMELSSLRSEDTAVYYCAREDSDFHDGHGHTLRGMFDYWGQGTLVTVSS |
| | VL reverted | QSVLTQPPSASGTPGQRVTISCSGSSSNIGSNYVYWYQQLPGTAPKLLIYRNNQRPSGVPDRFSGSKSGTSASLAISGLRSEDEADYYCAAWDDSLSGPVFGGGTKLTVL |
| VRC01[5] | VH reverted* | QVQLVQSGAEVKKPGASVKVSCKASGYTFTGYYMHWVRQAPGQGLEWMGWINPNSGGTNYAQKFQGRVTMTRDTSISTAYMELSRLRSDDTAVYYCARGKNSDYNWDFQHWGQGTLVTVSS |
| | VL reverted | EIVLTQSPATLSLSPGERATLSCRASQSVSSYLAWYQQKPGQAPRLLIYDASNRATGIPARFSGSGSGTDFTLTISSLEPEDFAVYYCQQYEFFGQGTKLEIK |
| 3BNC60[6] | VH reverted | QVQLVQSGAEVKKPGASVKVSCKASGYTFTGYYMHWVRQAPGQGLEWMGWINPNSGGTNYAQKFQGRVTMTRDTSISTAYMELSRLRSDDTAVYYCARERSDFWDFDLWGRGTLVTVSS |
| | VL reverted | DIQMTQSPSSLSASVGDRVTITCQASQDISNYLNWYQQKPGKAPKLLIYDASNLETGVPSRFSGSGSGTDFTFTISSLQPEDIATYYCQQYEFIGPGTKVDIK |
| NIH45-46[7] | VH reverted | QVQLVQSGAEVKKPGASVKVSCKASGYTFTGYYMHWVRQAPGQGLEWMGWINPNSGGTNYAQKFQGRVTMTRDTSISTAYMELSRLRSDDTAVYYCARGKYCTARDYYNWDFQHWGQGTLVTVSS |
| | VL reverted | EIVLTQSPATLSLSPGERATLSCRASQSVSSYLAWYQQKPGQAPRLLIYDASNRATGIPARFSGSGSGTDFTLTISSLEPEDFAVYYCQQYEFFGQGTKLEIK |
| 12A12[5] | VH reverted | QVQLVQSGAEVKKPGASVKVSCKASGYTFTGYYMHWVRQAPGQGLEWMGWINPNSGGTNYAQKFQGRVTMTRDTSISTAYMELSRLRSDDTAVYYCARDGSGDDTSWHFDPWGQGTLVTVSS |
| | VL reverted | DIQMTQSPSSLSASVGDRVTITCQASQDISNYLNWYQQKPGKAPKLLIYDASNLETGVPSRFSGSGSGTDFTFTISSLQPEDIATYYCAVLEFFGPGTKVEIKRTVAAPSV |
| PGV19[5] | VH reverted | QVQLVQSGAEVKKPGASVKVSCKASGYTFTGYYMHWVRQAPGQGLEWMGWINPNSGGTNYAQKFQGRVTMTRDTSISTAYMELSRLRSDDTAVYYCARMGAAREWDFQYWGQGTRVLVSS |
| | VL reverted | ESALTQPASVSGSPGQSITISCTGTSSDVGGYNYVSWYQQHPGKAPKLMIYEVSNRPSGVSNRFSGSKSGNTASLTISGLQAEDEADYYCSSYEFFGGGTKLTVLGQ |
| CH103[8] | VH reverted | QVQLQESGPGLVKPSETLSLTCTVSGGSISSYYWSWIRQPPGKGLEWIGYIYYSGSTNYNPSLKSRVTISVDTSKNQFSLKLSSVTAADTAVYYCASLPRGQLVNAYFDYWGQGTLVTVSS |
| | VL reverted | SYELTQPPSVSVSPGQTASITCSGDKLGDKYACWYQQKPGQSPVLVIYQDSKRPSGIPERFSGSNSGNTATLTISGTQAMDEADYYCQAWDSFSTFVFGTGTKVTVL |
| 3BC315[1] | VH reverted | QVQLVQSGAEVKKPGASVKVSCKASGYTFTGYYMHWVRQAPGQGLEWMGWINPNSGGTNYAQKFQGRVTMTRDTSISTAYMELSRLRSDDTAVYYCARPMRPVSHGIDYSGLFVFQFWGQGTMVTVSS |
| | VL reverted | TGSVTQSALTQPASVSGSPGQSITISCTGTSSDVGSYNLVSWYQQHPGKAPKLMIYEVSKRPSGVSNRFSGSKSGNTASLTISGLQAEDEADYYCCSYANYDKLIFGGGTKLTVLSQPKAAPSVTLFPPS |

* The same sequences are used in the knock-in mice as in the binding studies


1. Sliepen et al., 2015
2. Pancera et al., 2010
3. Bonsignori et al., 2011
4. Escolano et al., 2016
5. Jardine et al., 2013
6. Dosenovic et al., 2015
7. Scharf et al., 2013
8. Liao et al., 2013

**Table S2. Related to Figure 1A, B. Neutralization sensitivity of a panel of viruses to the inferred germline versions of PG9, PG16 and PGT145.** The TZM-bl cell assay was used to determine the percentage of neutralization at the maximum concentration of antibody. The ACS viruses are clinical isolates, BL035 and Q23 are Env-pseudotyped viruses and BG505 is a molecular clone (see SI Methods). The neutralization assays were performed in triplicate. The mean values, with standard deviations, are shown and ranged by color as indicated. The V2 sequence column shows the relevant sequences of residues 156 to 196 (HxB2 numbering system). The BG505 SOSIP.v4.1-GT1 sequence is indicated by the black arrow, the changes are highlighted in dark grey boxes/white characters, and the 7 amino-acid deletion is indicated by the gray shading over the dashed line. The origins of those changes are indicated by dashed boxes. The R178K change that was taken from elsewhere (Aussedat et al., 2013) is indicated with a shade of gray.

(table attached)

**Table S3. Related to Figure 1B. Relative binding of a panel of three gl-bNAbs and two bNAbs to BG505 SOSIP.664 variants in a D7324-capture ELISA using supernatants from transfected HEK293T cells.**

| Modifications introduced to BG505 SOSIP.664 | | | Germline[4] | | | Mature | |
|---|---|---|---|---|---|---|---|
| Stability[2] | V1V2-apex gl-bNAb Enhancement | CD4bs gl-bNAb enhancement | PG9 | VRC01 | PGV19 | 2G12 | PGT145 |
| - | - | - | - | - | - | +++++ | +++++ |
| A316W | - | - | - | - | - | +++++ | +++++ |
| A316W E64K | - | - | - | - | - | +++++ | +++++ |
| A316W | ΔRSNNSNK[3] | - | + | - | - | +++++ | +++++ |
| A316W | ΔRSNNSNK[3] | N462D | + | - | - | +++++ | +++++ |
| A316W | ΔRSNNSNK[3] | N276D | + | - | +/- | +++++ | +++++ |
| A316W | ΔRSNNSNK[3] | N276D N462D | + | - | + | +++++ | +++++ |
| A316W E64K | ΔRSNNSNK[3] | N276D N462D | + | - | + | +++++ | +++++ |
| A316W E64K | ΔRSNNSNK[3] | N276D N462D G471S | + | - | ++ | +++++ | +++++ |
| A316W E64K | ΔRSNNSNK[3] | N276D N462D N386D | + | - | ++ | +++++ | +++++ |
| A316W E64K | ΔRSNNSNK[3] | N276D N462D T278R | + | + | +++ | +++++ | +++++ |
| A316W E64K | ΔRSNNSNK[3] | N276D N462D T278R N386D G471S | + | ++ | ++++ | +++++ | +++++ |
| A316W E64K | ΔRSNNSNK[3] K169R Y173H S174A R178K V181I Q183P | N276D N462D T278R N386D G471S S199A | ++ | +++ | ++++ | +++++ | +++++ |
| A316W E64K | ΔRSNNSNK[3] K169R Y173H S174A R178K V181I Q183P | N276D N462D T278R N386D G471S S199A | ++ | +++ | ++++ | +++++ | +++++ |
| A316W E64K | ΔRSNNSNK[3] K169R Y173H S174A R178K V181I Q183P G188N N189T 190S | N276D N462D T278R N386D G471S S199A | ++++ | ++++ | ++++ | +++++ | +++++ |

1. Unpurified HEK293T cell culture supernatant.
2. See de Taeye et al. (2015).
3. Seven amino-acid deletion between residues 185e and 190 (HxB2 numbering).
4. See Table S1.

**Table S4. Related to Figure 1B. Relative binding of panel of three gl-bNAbs and two bNAbs to BG505 SOSIP.664 variants in a Ni-NTA/His-tag capture ELISA using supernatants from transfected HEK293T cells.**

| Modifications introduced to BG505 SOSIP.664 | | | Germline[4] | | | Mature | |
|---|---|---|---|---|---|---|---|
| Stability[2] | V1V2-apex gl-bNAb Enhancement | CD4bs gl-bNAb enhancement | PG9 | VRC01 | PGV19 | 2G12 | PGT145 |
| - | - | - | - | - | - | +++++ | +++++ |
| A316W | - | - | - | - | - | +++++ | +++++ |
| A316W E64K | - | - | - | - | - | +++++ | +++++ |
| A316W E64K | ΔRSNNSNK[3] | N276D N462D | + | - | + | +++++ | +++++ |
| A316W E64K | ΔRSNNSNK[3] | N276D N462D G471S | + | - | ++ | +++++ | +++++ |
| A316W E64K | ΔRSNNSNK[3] | N276D N462D N386D | + | - | ++ | +++++ | +++++ |
| A316W E64K | ΔRSNNSNK[3] | N276D N462D T278R | + | ++ | +++ | +++++ | +++++ |
| A316W E64K | ΔRSNNSNK[3] K169R Y173H S174A R178K V181I Q183P G188N N189T 190S | N276D N462D T278R N386D G471S S199A | +++ | ++++ | ++++ | +++++ | +++++ |

1. Unpurified HEK293T cell culture supernatant.
2. See de Taeye et al. (2015).
3. Seven amino-acid deletion between residues 185e and 190 (HxB2 numbering).
4. See Table S1.

**Table S5. Related to Figure 1B. Relative binding of panel of three gl-bNAbs and two bNAbs to BG505 SOSIP.664 variants by Ni-NTA/His-tag capture ELISA using affinity chromatography purified trimers.**

| Modifications introduced to BG505 SOSIP.664 | | | Mermline[4] | | | Mature | |
|---|---|---|---|---|---|---|---|
| **Stability[2]** | **V1V2-apex gl-bNAb Enhancement** | **CD4bs gl-bNAb enhancement** | **PG9** | **VRC01** | **PGV19** | **2G12** | **PGT145** |
| | | | ++ | - | - | +++++ | ++++ |
| A316W | - | - | ++ | - | - | +++++ | +++++ |
| A316W E64K | - | - | +++ | - | - | +++++ | +++++ |
| A316W E64K | ΔRSNNSNK[1] | N276D N462D | +++ | - | ND | +++++ | +++++ |
| A316W E64K | ΔRSNNSNK[1] | N276D N462D G471S | +++ | + | ND | ++++ | ++++ |
| A316W E64K | ΔRSNNSNK[1] | N276D N462D N386D | +++ | + | ND | ++++ | ++++ |
| **A316W E64K** | **ΔRSNNSNK[1]** | **N276D T278R** | +++ | +++ | +++++ | +++++ | +++++ |
| A316W E64K | ΔRSNNSNK[1] | N276D T278R N462D | +++ | ++++ | +++++ | +++++ | +++++ |
| A316W E64K | ΔRSNNSNK[1] K169R Y173H S174A R178K V181I Q183P G188N N189T 190S | N276D N462D T278R N386D G471S S199A | +++++ | +++++ | +++++ | +++++ | +++++ |

ND. Not determined.
1. Trimers purified with affinity chromatography using a PGT145 column.
2. See de Taeye et al. (2015).
3. Seven amino-acid deletion between residues 185e and 190 (HxB2 numbering).
4. See Table S1.

**Table S6. Related to Figure 1E. Percentage of $Man_{5-9}GlcNAc_2$ glycans (M5-M9) as the proportion of the total glycan population.**

| % / Molecule | M5 | M6 | M7 | M8 | M9 | Sum |
|---|---|---|---|---|---|---|
| **BG505 SOSIPv.4.1-GT1** | 7 | 5 | 9 | 22 | 17 | **59** |
| **BG505 SOSIP.v4.1** | 8 | 5 | 7 | 21 | 23 | **64** |
| **BG505 SOSIP.664** | 8 | 5 | 8 | 19 | 25 | **66** |

**Table S7. Related to Figure 2B. SPR analysis of the mature and germline versions of a panel of bNAbs to SOSIP.664 trimer variants.**

**(table attached)**

**Table S8. Related to Figs. 3 and 4. X-ray data collection and refinement statistics.**

| Data collection | BG505 SOSIP.v4.1-GT1-N137A-9H+109L + 35O22 |
|---|---|
| Beamline | APS 23-ID-D |
| Wavelength (Å) | 1.033 |
| Space group | $P6_3$ |
| Unit cell (Å) | a = b=128.0, c=316.1 |
| Resolution (Å) | 50.0-3.2 (3.26-3.20) [a] |
| Observations | 610,919 |
| Unique reflections | 47,220 (2,375) [a] |
| Redundancy | 12.9 (13.1) [a] |
| Completeness (%) | 100 (100) [a] |
| $<I/\sigma_I>$ | 11.0 (1.0) [a] |
| $R_{sym}$ [b] | 0.11 (1.00) [a] |
| $R_{pim}$ [c] | 0.08 (0.77) [a] |
| $CC_{1/2}$ [d] | 0.89 (0.52) |
| **Refinement statistics** | |
| Resolution (Å) | 49.4-3.2 |
| Reflections (work) | 44,674 |
| Reflections (test) | 2,409 |
| $R_{cryst}$ (%) [e] | 27.2[c] (42.7) [a] |
| $R_{free}$ (%) [f] | 28.5[d] (45.5) [a] |
| Average B-value (Å$^2$) | |
| All proteins | 126 |
| gp120 | 106 |
| gp41 | 115 |
| 9H+109L ($V_H/V_L$) | 122 |
| 9H+109L ($C_L/C_H1$) | 207 |
| 35O22 ($V_H/V_L$) | 122 |
| 35O22 ($C_L/C_H1$) | 207 |
| Glycans | 99 |
| Wilson B-value (Å$^2$) | 97 |
| **RMSD from ideal geometry** | |
| Bond length (Å) | 0.005 |
| Bond angles (°) | 0.974 |
| **Ramachandran statistics (%)** [g] | |
| Favored | 96.3 |
| Outliers | 0.1 |
| PDB ID | XXXX |

[a]Numbers in parentheses refer to the highest resolution shell.

[b]$R_{sym} = \Sigma_{hkl}\Sigma_i \mid I_{hkl,i} - <I_{hkl}> \mid / \Sigma_{hkl}\Sigma_i I_{hkl,I}$, where $I_{hkl,i}$ is the scaled intensity of the $i^{th}$ measurement of reflection h, k, l, $<I_{hkl}>$ is the average intensity for that reflection, and $n$ is the redundancy (Weiss and Hilgenfeld, 1997). .

[c]$R_{pim}$ is a redundancy-independent measure of the quality of intensity measurements. $R_{pim} = \Sigma_{hkl} (1/(n-1))^{1/2} \Sigma_i \mid I_{hkl,i} - <I_{hkl}> \mid / \Sigma_{hkl} \Sigma_i I_{hkl,I}$, where $I_{hkl,i}$ is the scaled intensity of the $i^{th}$ measurement of reflection h, k, l, $< I_{hkl} >$ is the average intensity for that reflection, and $n$ is the redundancy.

[d]$CC_{1/2}$ = Pearson Correlation Coefficient between two random half datasets.

[e]$R_{cryst} = \Sigma_{hkl} \mid F_o - F_c \mid / \Sigma_{hkl} \mid F_o \mid$ x 100

[f]$R_{free}$ was calculated as for $R_{cryst}$, but on a test set comprising 5% of the data excluded from refinement.

[g]Calculated using MolProbity (Chen et al., 2010).

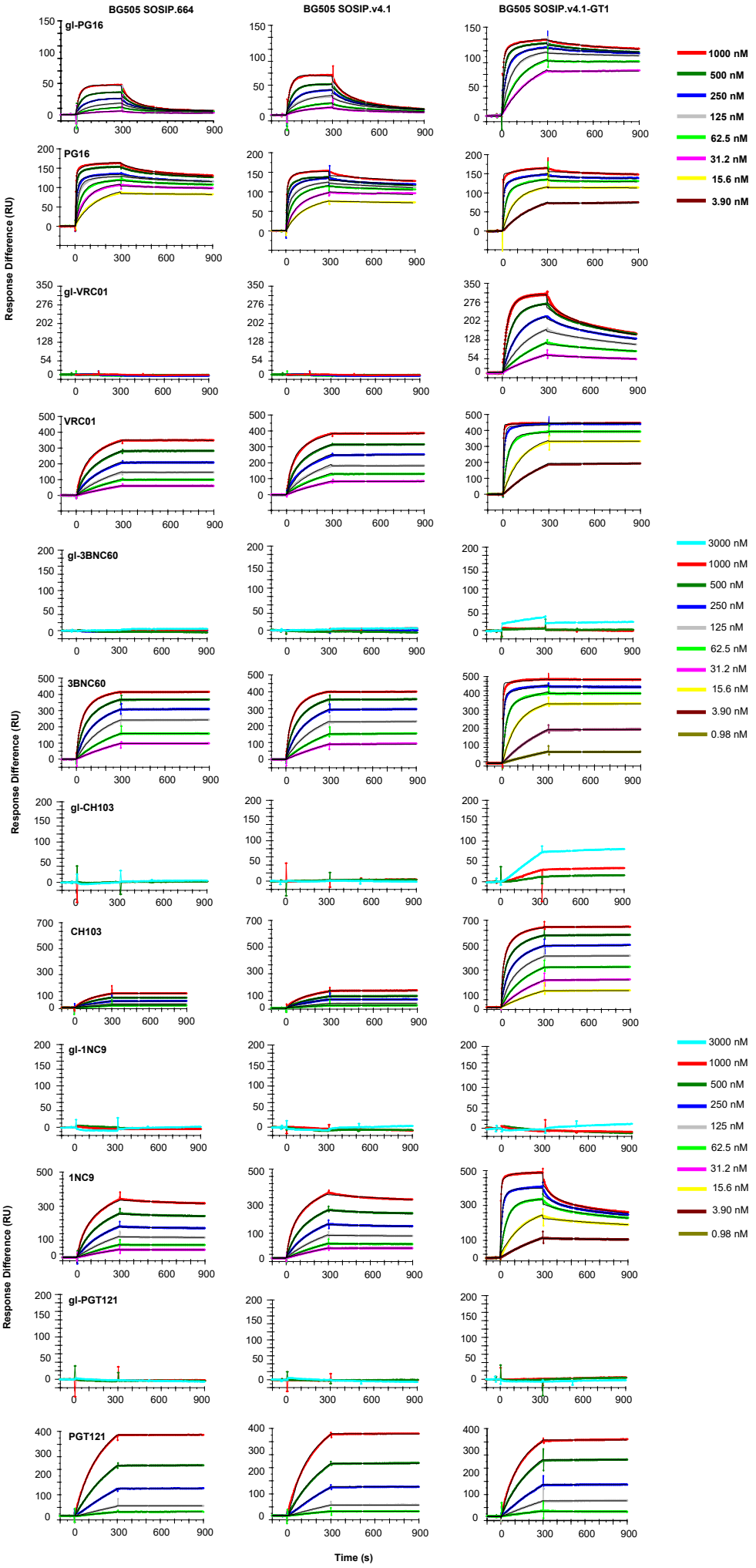
BG505 SOSIP.664
BG505 SOSIP.v4.1
BG505 SOSIP.v4.1-GT1
gl-PG16
PG16
gl-VRC01
VRC01
gl-3BNC60
3BNC60
gl-CH103
CH103
gl-1NC9
1NC9
gl-PGT121
PGT121
1000 nM
500 nM
250 nM
125 nM
62.5 nM
31.2 nM
15.6 nM
3.90 nM
3000 nM
0.98 nM
Response Difference (RU)
Time (s)

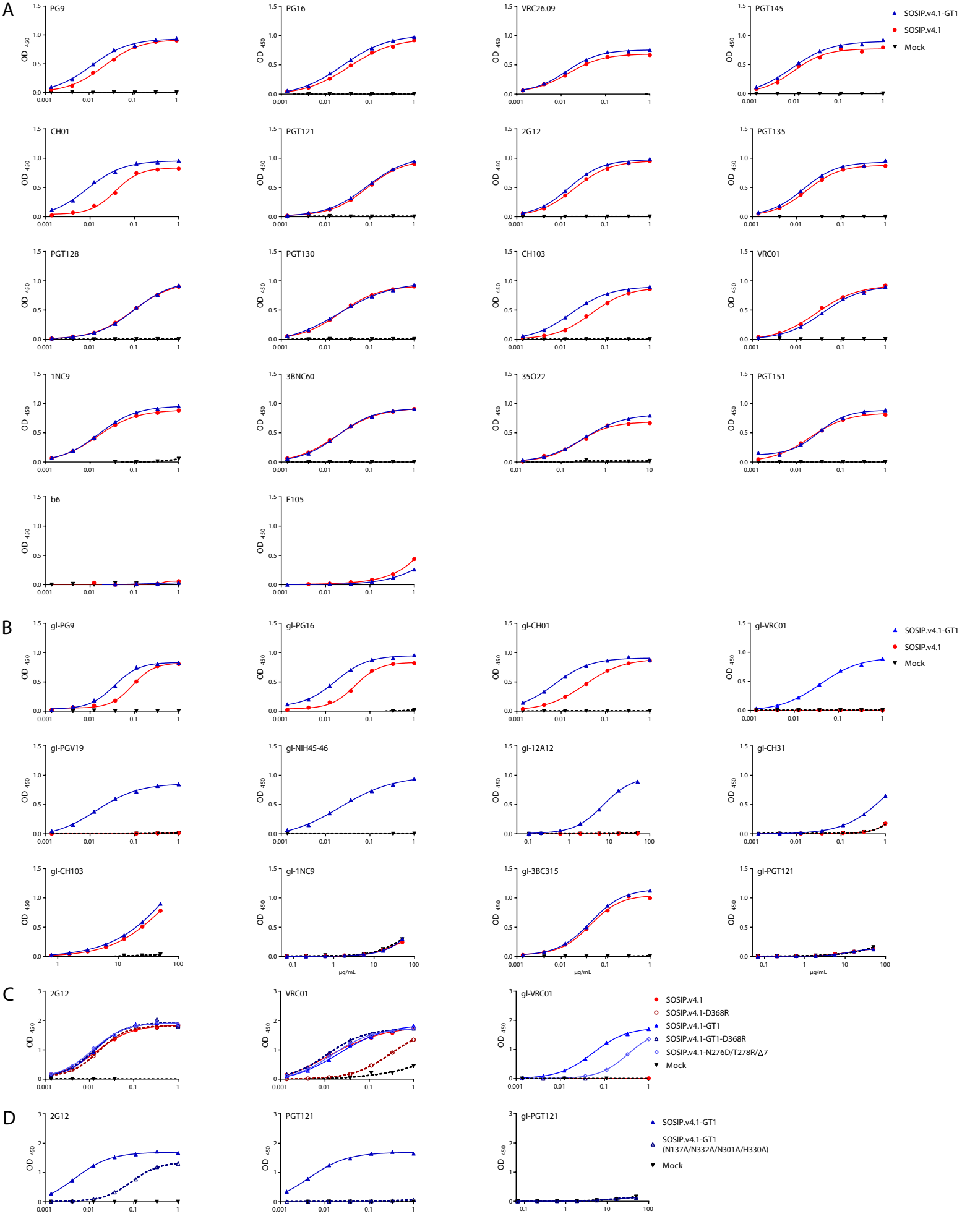
A
PG9
PG16
VRC26.09
PGT145
CH01
PGT121
2G12
PGT135
PGT128
PGT130
CH103
VRC01
1NC9
3BNC60
35O22
PGT151
b6
F105
SOSIP.v4.1-GT1
SOSIP.v4.1
Mock
B
gl-PG9
gl-PG16
gl-CH01
gl-VRC01
gl-PGV19
gl-NIH45-46
gl-12A12
gl-CH31
gl-CH103
gl-1NC9
gl-3BC315
gl-PGT121
μg/mL
C
2G12
VRC01
gl-VRC01
SOSIP.v4.1
SOSIP.v4.1-D368R
SOSIP.v4.1-GT1
SOSIP.v4.1-GT1-D368R
SOSIP.v4.1-N276D/T278R/Δ7
Mock
D
2G12
PGT121
gl-PGT121
SOSIP.v4.1-GT1
SOSIP.v4.1-GT1 (N137A/N332A/N301A/H330A)
Mock
OD 450